AD-A052 356 WESTINGHOUSE RESEARCH AND DEVELOPMENT CENTER PITTSBU--ETC F/G 9/1
EVALUATION OF SULFOSALTS.(U)
OCT 77 T J ISAACS, R W WEINERT, J MURPHY F19628-76-C-0158
UNCLASSIFIED RADC-TR-77-367 NL

1 OF
AD
A052 356

END
DATE
FILMED
5-78
DDC

(2)

RADC-TR-77-367
Final Technical Report
October 1977

EVALUATION OF SULFOSALTS

Westinghouse Research & Development Center

Approved for public release; distribution unlimited

This research was sponsored by the Defense Advanced Research Projects Agency (DOD) ARPA Order No. 3151

ROME AIR DEVELOPMENT CENTER
AIR FORCE SYSTEMS COMMAND
GRIFFISS AIR FORCE BASE, NEW YORK 13441

ARPA Order Number	Contract Number
3151	F19628-76-C-0158
Program Code Number	Principal Investigator and Phone Number
6D10	Thelma J. Isaacs (412) 256-3557
Name of Contractor	RADC Project Scientist and Phone Number
Westinghouse R&D Center	Dr. Stanley Dickinson (ESM) (617) 861-2211
Effective Date of Contract	
April 15, 1976	Contract Expiration Date
	October 15, 1977

This report has been reviewed by the RADC Information Office (OI) and is releasable to the National Technical Information Service (NTIS). At NTIS it will be releasable to the general public, including foreign nations.

Stanley K. Dickinson

STANLEY K. DICKINSON
Contract Monitor
Solid State Sciences Division

Unclassified @Final rept.

SECURITY CLASSIFICATION OF THIS PAGE (When Data Entered)

(19) **REPORT DOCUMENTATION PAGE**

READ INSTRUCTIONS BEFORE COMPLETING FORM

(18) 1. REPORT NUMBER: RADC-TR-77-367	2. GOVT ACCESSION NO. / 3. RECIPIENT'S CATALOG NUMBER
(6) 4. TITLE (and Subtitle): EVALUATION OF SULFOSALTS	5. TYPE OF REPORT & PERIOD COVERED: Final Report 4-15-76 - 10-15-77
	6. PERFORMING ORG. REPORT NUMBER
(10) 7. AUTHOR(s): T. J. Isaacs, J. Murphy, R. W. Weinert, J. P. McHugh	(15) 8. CONTRACT OR GRANT NUMBER(s): F19628-76-C-0158
9. PERFORMING ORGANIZATION NAME AND ADDRESS: Westinghouse Research & Development Center, 1310 Beulah Road, Pittsburgh, PA 15235	10. PROGRAM ELEMENT, PROJECT, TASK AREA & WORK UNIT NUMBERS: 61101E, (16) 3151 T&WU n/a
11. CONTROLLING OFFICE NAME AND ADDRESS: Deputy for Electronic Technology (RADC), Hanscom AFB, Massachusetts 01731, Monitor/Stanley Dickinson/ETSP	(11) 12. REPORT DATE: Oct 1977; 13. NUMBER OF PAGES: (12) 87 P.
(9) 14. MONITORING AGENCY NAME & ADDRESS (if different from Controlling Office): Final technical rept. 15 Apr 76-15 Oct 77	15. SECURITY CLASS. (of this report): Unclassified; 15a. DECLASSIFICATION/DOWNGRADING SCHEDULE

16. DISTRIBUTION STATEMENT (of this Report)

Approved for public release; distribution unlimited.

17. DISTRIBUTION STATEMENT (of the abstract entered in Block 20, if different from Report)

18. SUPPLEMENTARY NOTES

Sponsored by Defense Advanced Research Projects Ag ency (DOD)
ARPA Order No. 3151

19. KEY WORDS (Continue on reverse side if necessary and identify by block number)

zero temperature coefficient of delay directions, thallium vanadium sulphide, furnace and control systems, surface-wave filter, bulk-wave resonator, crystal growth, optimum composition, dielectric constant, piezoelectric constant, thallium tantalum sulphide

20. ABSTRACT (Continue on reverse side if necessary and identify by block number)

Phase equilibria studies conducted in the system Tl-V-S around the composition Tl_3VS_4 indicate that this compound may melt incongruently or alternatively, that there may be a eutectic very near it. The relations are not as yet fully understood. Nevertheless, we can see from either interpretation reasons for our problems in synthesis and crystal growth. We have learned to grow good quality crystals by having the reactant composition vanadium-poor; slow growth rates and very steep thermal gradients also were necessary.

DD FORM 1 JAN 73 1473 EDITION OF 1 NOV 65 IS OBSOLETE

UNCLASSIFIED

SECURITY CLASSIFICATION OF THIS PAGE (When Data Entered)

376 625 i JOB

20. (cont.)

We have completed two parts of our studies on crystal growth parameters, rates of growth and gradient.

Initial studies were performed to understand phase relations in the system Tl-Ta-Se around the composition Tl_3TaSe_4.

We have taken steps to minimize the silica-glass container problem, but we have not been able to eliminate it.

The material constants of Tl_3VS_4 and the temperature coefficients have been measured, and the final results are presented. Some temperature stable cuts for surface wave propagation have been investigated, and a S.A.W. filter has been fabricated and tested. Our work on surface waves has also included modifying the theoretical calculations to account for bulk wave generation and leaky surface waves.

TABLE OF CONTENTS

TABLE OF CONTENTS (Cont.)

LIST OF ILLUSTRATIONS

LIST OF TABLES

LIST OF PLATES

EVALUATION OF SULFOSALTS

Final Report
Contract No. F19628-76-C-0158

1. INTRODUCTION

1.1 Program Objectives

The program had two principal objectives, one of which was to determine the optimum conditions for fabrication of reproducible, high-quality crystals of Tl_3VS_4, and possibly other members of the Tl_3BX_4 family of materials. The other was to determine directions in these crystals having zero temperature coefficients of delay (ZTCD) for surface acoustic waves, and to assess which of these directions possesses the best combination of velocity, k^2, and power flow angle for device applications. New determinations of physical parameters (attenuation, velocities, k^2) were to be made on improved crystals.

In addition, the effects of wider temperature ranges and higher order temperature coefficients of velocity were to be examined. Hall measurements also were to be made. A bandpass filter was to be fabricated to demonstrate the applicability of these materials for surface-wave devices.

1.2 General Approach

The approach adopted for the determination of the optimum composition for crystal growth was to study phase relations around the stoichiometric composition in the ternary system Tl-V-S. The methods employed included thermal heating and cooling curves, quenching experiments, and directional solidification experiments.

Data from these experiments were used to understand and optimize crystal growth.

A computer program was developed to enable us to perform theoretical searches for ZTCD directions, given a selected set of parameters. This program also gives information on coupling, power-flow angle and possible "leakiness" in these directions. Experimental verification of some of these directions was undertaken.

1.3 Summary

Phase equilibria studies conducted in the system Tl-V-S around the composition Tl_3VS_4 indicate that this compound may melt incongruently or alternatively, that there may be a eutectic very near it. The relations are not as yet fully understood. Nevertheless, we can see from either interpretation reasons for our problems in synthesis and crystal growth. We have learned to grow good quality crystals by having the reactant composition vanadium-poor; slow growth rates and very steep thermal gradients also were necessary.

We have completed two parts of our studies on crystal growth parameters, rates of growth and gradient.

Initial studies were performed to understand phase relations in the system Tl-Ta-Se around the composition Tl_3TaSe_4.

We have taken steps to minimize the silica-glass container problem, but we have not been able to eliminate it.

The material constants of Tl_3VS_4 and the temperature coefficients have been measured, and the final results are presented. Some temperature stable cuts for surface wave propagation have been investigated, and a S.A.W. filter has been fabricated and tested. Our work on surface waves has also included modifying the theoretical calculations to account for bulk wave generation and leaky surface waves.

2. TECHNIQUES OF MATERIALS PREPARATION, PHASE EQUILIBRIA STUDIES, AND CRYSTAL GROWTH

2.1 Techniques of Materials Preparation

The reactant materials used for phase equilibria studies and for crystal growth were prepared from the high-purity elements (> 99.999 wt.% purity) Tl, V, Ta, S, and Se. As Tl and V tend to oxidize readily, considerable care was taken to ensure that the surfaces of these elements were entirely free from oxide contamination. The oxide coating the Tl was removed by first heating the ingot in deionized water, followed by ultrasonic agitation and a final rinse in deionized water. The beaker of water containing the cleaned ingot was placed into a glove bag under nitrogen atmosphere. The ingot was removed from the water and blown dry using "Dust-Off". It was then set into an ampoule which was placed on the vacuum system, and the ampoule alternately evacuated and backfilled with argon a number of times, and then left under high vacuum for approximately 30 minutes to ensure thorough drying. The Tl was placed in a pre-weighed bottle in the N_2-filled glove bag, the tightly-fitting stopper inserted into the bottle, and weighed outside the glove bag. The container and its contents were returned to the glove bag, and the ingot then placed into a silica-glass tube which was immediately evacuated.

The oxide coating the V was removed by use of a weak nitric acid bath. This was followed by thorough washing with deionized water. It was dried in a glove bag under N_2, and weighed quickly in air. The V was then returned immediately to the glove bag. Tantalum was cleaned of its oxide coating in a bath consisting of 5 parts H_2SO_4, 2 parts HNO_3 and 2 parts HF. It was then washed in deionized water and handled in the same way as vanadium.

Sulphur and selenium require no special handling, and were weighed in air and then placed into the silica-glass tubes via the N_2-filled glove bag. The tubes containing these three elements were sealed under a pressure of $<5 \times 10^{-6}$ torr, and placed in horizontal split furnaces which had been preheated to between 500-700°C to encourage rapid reaction and lessen the possibility of explosion. After reaction occurred, the temperatures were raised to approximately 1000°C and held there for several hours. The temperature was then lowered to ∿750°C and the ampoules containing the molten material held for several days, with intermittant vigorous shaking to promote homogeneity. When the reactant material was to be used for crystal growing or for determination of heating and cooling curves, it was cooled slowly to room temperature. When it was to be used for quench-type studies, it was quickly chilled in an ice water bath.

2.2 Techniques of Phase Diagram Study

Two techniques were used for the phase diagram study, thermal analysis and quench-type (or silica-tube) experiments. Both types of experiments were conducted in sealed, initially evacuated, silica-glass containers, which are well-suited for reactions among chalcogenide compounds of low or moderate melting points because they are inert, and because they constitute sealed containers for volatile components such as sulphur.

The same high-purity materials were used in this part of the work as are described in Section 2.1, and the methods of cleaning the surfaces of Tl and V were identical with those described in that section.

The experimental system for thermal analysis consisted of a well-lagged furnace, a temperature control system, and a strip chart recorder which produced a direct plot of sample temperature as a function of time. The sample material was contained in silica-glass ampoules containing a well into which a chromel-alumel thermocouple was inserted. The thermocouple was tied to the ampoule with nichrome wire, and then passed out of the furnace through a narrow opening. The ampoule itself

was seated vertically in a ceramic block. The thermocouple cold junction was placed in an ice bath. Most of the data were collected from cooling curves, but as there was considerable supercooling, we also obtained information from heating curves. The rates of cooling which we used varied from as fast as 1°C/min to a much slower speed of 10°C/hour. Most of the experiments were run at the slower rates as the problem of supercooling was then less severe. The sample was often reheated and cooled a number of times to obtain better information on the shape and temperature of thermal arrests. In this set of experiments, we concentrated on the liquidus part of the phase diagram as we wanted to determine the maximum-melting composition, which is the one best suited for crystal growth.

A new thermal analysis technique was recently developed on another project at our laboratories, and we performed a number of experiments on it this summer to try to reconcile ambiguous data. This method employs a small furnace which contains little mass, and may be regarded more as a radiant heater for the silica-glass ampoule than as a furnace proper. The system also contained a temperature control system and a strip chart recorder which gave a direct plot of sample temperature with time. Small silica-glass ampoules having a thermocouple well in the bottom and a bulb protruding from the neck portion for seeds were used to house the sample. The design of this system, which is described in detail elsewhere,[1] permits thermal homogeneity to be obtained at a faster rate than the larger system we had been using. This had the advantage not only of speeding up the experimental work, but also of reducing some possible sources of error, particularly in a complex system such as Tl-V-S. It appeared to lessen the problem of segregation of secondary phases which reduced the scatter of data points. It also permitted seeding of melts where supercooling was a problem so that we could attain greater accuracy in determining freezing point temperatures.

Quench-type experiments were used in conjunction with thermal analysis to aid in the determination of the best composition for growing crystals. In these studies, reactant materials (typically 200 mg) were

weighed in the desired proportions, sealed under vacuum in silica-glass containers and heated for lengths of time necessary to obtain equilibrium assemblages for a given temperature. They were then chilled to room temperature by dropping the hot ampoule into a container of ice-water immediately upon removal from the furnace. Phases were identified using standard microscope and x-ray powder diffraction methods.

2.3 Crystal Growth

2.3.1 Basic Overview

Crystals of these materials were grown using the Stockbarger technique. Requirements for growing crystals of sulfosalt-type materials include slow growth rates (5-20 mm/day) and steep temperature gradients (5-15°C/mm) at the solid-liquid interface in the crystal-growing furnace.

Portions of polycrystalline reactant material were sealed under about 0.8 atm pressure of pure argon into silica-glass "crystal-growing" tubes which contained a pointed protrusion at the bottom to initiate single crystal growth. The argon pressure in the tube suppressed the presence of vapor during the run.

Cylindrical silica-glass furnaces were initially used for our crystal growing. Each furnace consisted of two heated zones separately controlled by variacs: an upper high-temperature zone and a lower low-temperature zone. The temperature gradient at the solid-liquid interface could be varied by adjusting the voltages to the two windings. As the crystal-growth tubes containing the melts were dropped slowly through the furnace, the melts crystallized when the temperature reached that of the solidification (melting) point. The grown crystal was allowed to anneal at the temperature of the lower furnace (usually set at about half the melting temperature), and was then cooled to room temperature over a period of two to three days.

Although these furnaces had been used successfully in growing sulfosalt crystals of high quality, they have deficiencies which tend to be more pronounced in effect when we are dealing with materials having steep liquidus curves around the maximum melting composition and/or eutectic interference problems. They are uninsulated and have the temperature "controlled" directly by variacs, which makes crystals growing in them more sensitive to changes in ambient temperature and in line voltages. Both of these problems can affect the interface gradient and its position in the furnace. Some of the adverse results include banding, precipitation of other phases, and the development of polycrystallinity due to breakdown at the solid-liquid interface.

Studies of crystals of Tl_3VS_4 grown in these systems indicated that these shortcomings were having a deleterious effect on the quality of our crystals, illustrated by plate 1. Phase diagram investigations into the system Tl-V-S (discussed in Section 3) tended to confirm this conclusion. As a result, a furnace system was designed to provide a satisfactory environment for high quality growth. This controlled growth furnace was used particularly in connection with our studies of the effects of crystal growth parameters (e.g., growth rate, gradient, rate of cooling) on crystal quality. Crystals for general use were still grown in the old system.

Plate 1

207057-96
Tl_3VS_4
Showing banding
Magnification = 100X

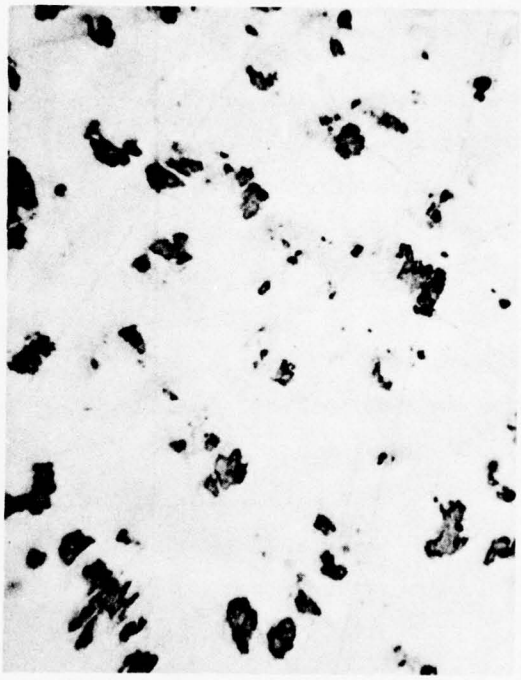

207057-153
$Tl_{3.01}V_{0.99}S_{3.98}$
Magnification = 200X

Photographs of sections of two crystals
illustrating inclusions and banding.

2.3.2 Controlled Growth Furnace

The complexities associated with many ternary chalcogenides, including Tl_3VS_4, and their resulting sensitivity to growth conditions, mentioned above, impose a number of requirements on a crystal growth furnace.

1. Both long-term and short-term temperature stability are needed. Temperature fluctuations produce perturbations in growth rate, which can in turn produce compositional inhomogeneities which seriously degrade crystal quality.
2. A steep gradient at the growth interface is desirable in order to provide increased homogeneity in the melt.
3. Slow and uniform growth rates allow diffusion of impurities away from the solid-liquid interface to improve homogeneity, provided requirement 1 is satisfied.
4. Susceptibility to damage from thermal stress requires that the grown crystal be cooled slowly.
5. In order to evaluate meaningfully the effect of small compositional changes on crystal quality, growth conditions must be closely reproducible from one run to the next.

In an attempt to meet the above requirements, the furnace shown schematically in Fig. 1 was designed and constructed along with a suitable control system. The furnace consists of two independently controlled heaters whose temperatures are adjusted to provide the desired gradient between them. Each heater zone is lined with a massive nickel heat leveler which helps linearize the temperature along that zone, sharpens the gradient between the zones, and provides a large thermal mass to aid in temperature stability. Chromel-alumel control thermocouples are positioned against the heater windings for maximum sensitivity.

The mechanism used to lower the crystal growth ampoule through the gradient consists of a screw and ball nut arrangement which converts the output of the synchronous motor and gear box to a smooth linear drive. The drop rate can be varied over a wide range of fixed gear ratios.

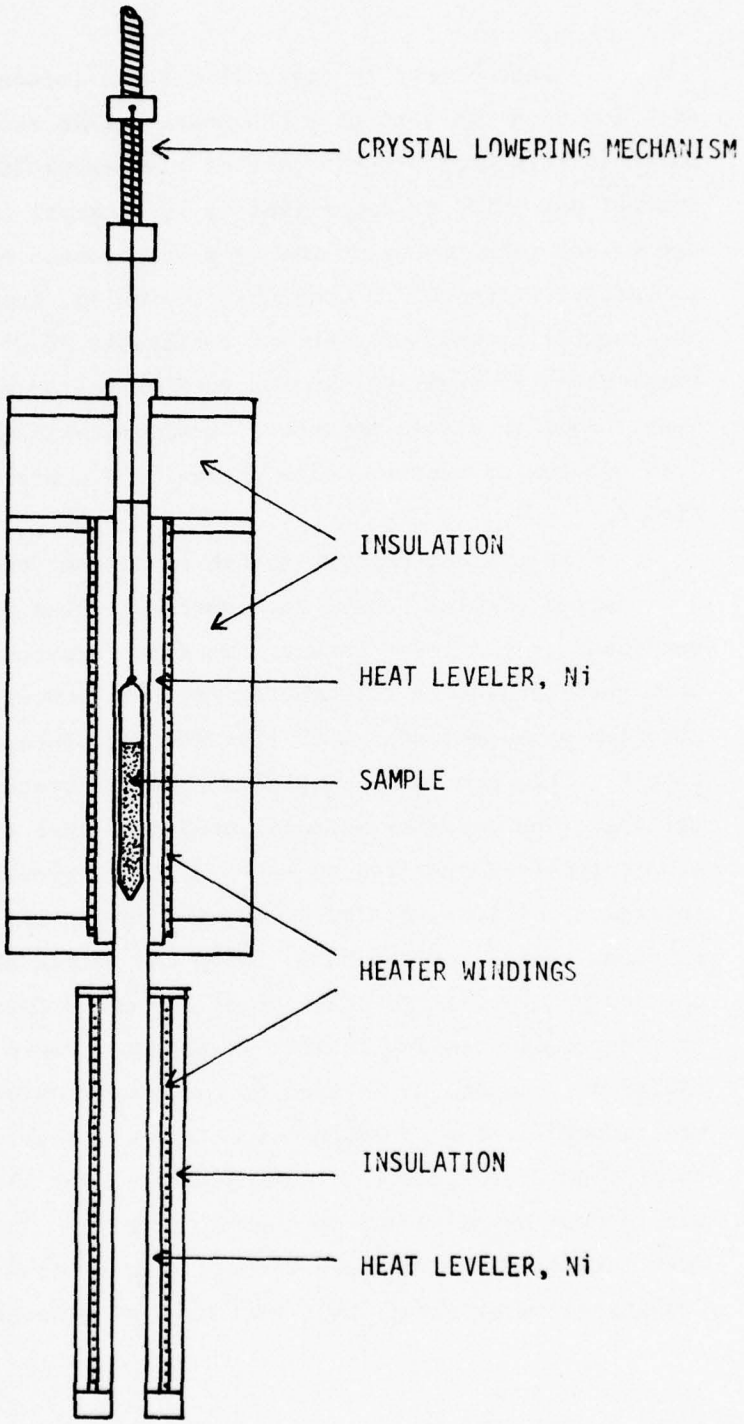

SULFOSALT CRYSTAL GROWING FURNACE

Fig. 1.

Each heater is controlled by an independent system. The control unit for each consists of a L&N model W AZAR recorder with a CAT controller which in turn controls the gate of a Research Inc. Model C32 phaser. Control set point is determined by an external ten turn helipot which can be set manually or driven by a synchronous motor and gear box through a clutch for controlled cooling. Typically, temperature as measured by the control thermocouple output oscillates $\pm$0.05°C about the set point. Temperature fluctuations in the working region of the furnace should be less. This is also a measure of reproducibility of temperature settings from one run to another. The furnace and control system are shown in Fig. 2.

A typical crystal growth experiment proceeded as follows. The pre-reacted sample, sealed in a quartz crystal growth ampoule, was suspended in the lower zone of the cold furnace. Both furnace zones were then brought up to temperature. The ampoule was then moved gradually into the upper hot zone such that melting proceeded from the top of the sample. This procedure prevented possible cracking of the ampoule during melting. The ampoule was positioned such that the bottom tip of the sample remained unmelted so as to nucleate growth. When steady state thermal conditions were achieved, the sample was lowered through the gradient at the desired rate. When the entire ampoule had passed into the lower zone, the recorder spans and set points were adjusted so that the controlled cooling to room temperature could be carried out without additional adjustment of span or zero suppression. The degree of control was reduced during cooldown but, since the sample was solid, this caused no problems, provided the cooling process was slow enough to prevent the sample from cracking due to thermal strains. The thermal mass of the heat leveler damped out minor short term fluctuations which might occur. Cooling rates of about 100°C per day were generally used.

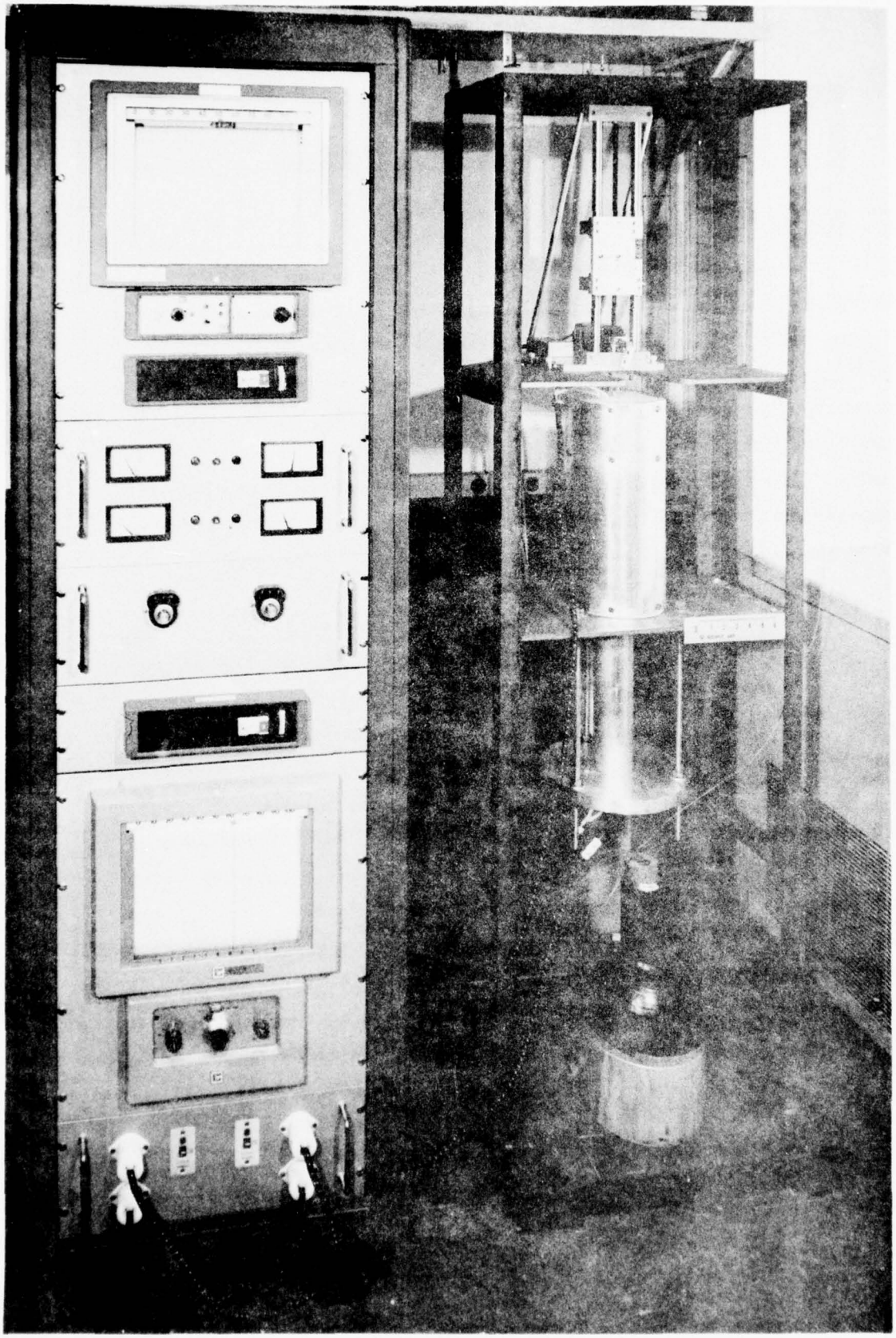

Fig. 2 New semi-automated two-zone furnace and control system

3. COMPOSITION AND CRYSTAL GROWTH STUDIES

3.1 Compounds in the System Tl-V-S

The compositions of compounds in the system Tl-V-S can be described in terms of a phase diagram (Fig. 3) in which compositions of many known binary and ternary compounds are plotted. There are four phases along the binary Tl-S, and a large number reported along the binary V-S, of which five are shown on the diagram. It must be noted that the existence of a compound of composition V_2S_5 is problematical. The V-S binary has compounds with large ranges of nonstoichiometric compositions, and the compositions given here are approximations. There are three ternary compounds, Tl_3VS_4, TlV_5S_8, and $Tl_xV_6S_8$ ($X = 0.05 - 0.8$).

3.2 Study of Phase Relations in the System Tl-V-S

In studies of phase relations in ternary systems, it is often found that ternary compounds lie on or near composition joins connecting two compounds in two of the binary systems. When all the equilibrium tie lines lie in the plane of the join, then the join may be treated as pseudobinary, i.e., a two-component system. Even if the join is not a true pseudobinary, it is convenient to use it as a basis of gathering data on phase relations near the compound of interest. Our approach to the problem of determing the best composition for growth of reproducible high-quality crystals of Tl_3VS_4 was to study phase relationships along selected joins to try to determine maximum melting composition, locations of eutectics, solid solution, possible peritectics, and secondary solid phases, particularly near this composition.

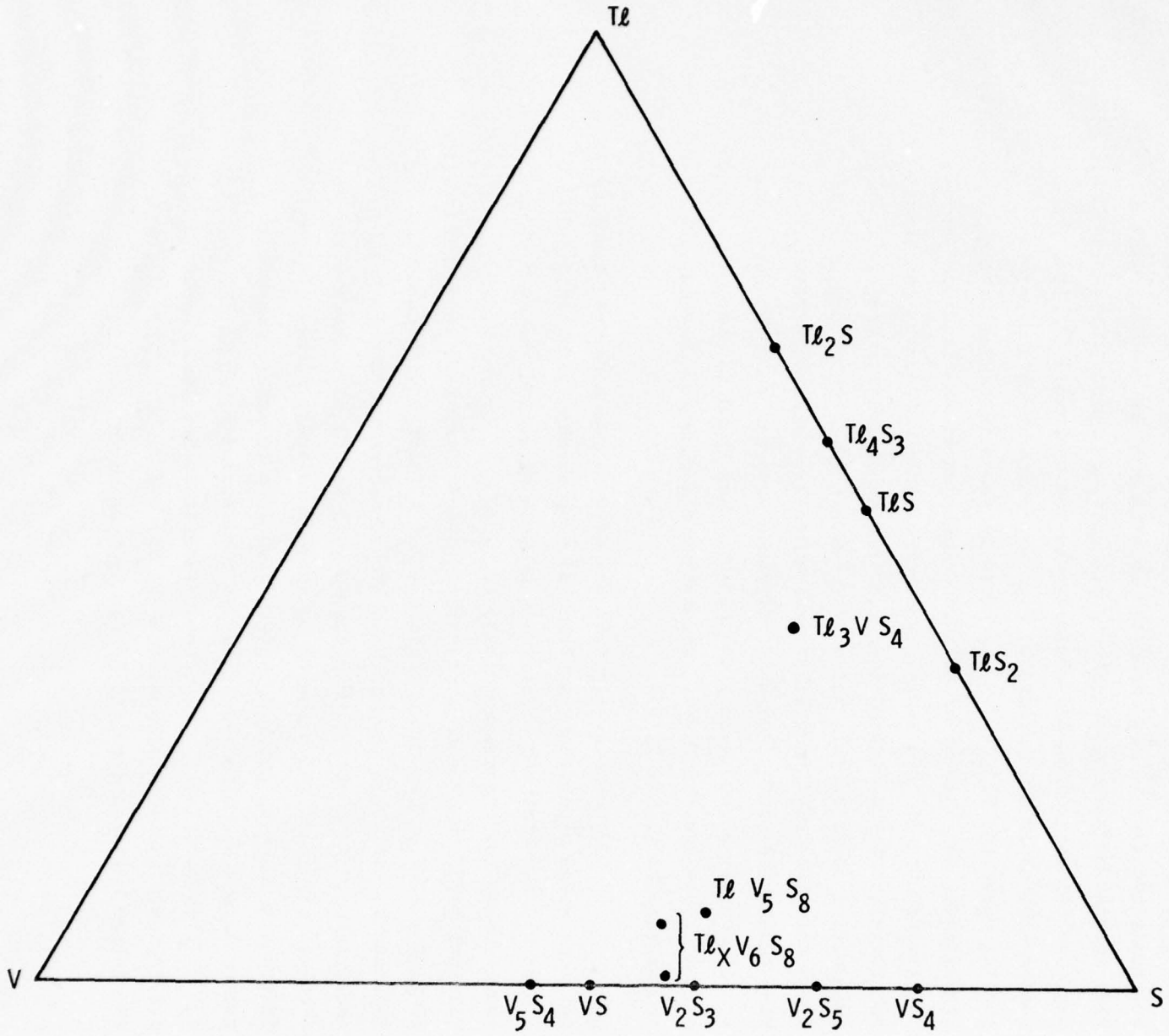

Fig. 3 — Phases in the system Tℓ-V-S

Our first set of experiments centered on the join Tl_2S-V_2S_5, which was selected on the basis of earlier work in other sulfosalt systems.[2,3] We found the relations to be complex, with a wide scatter of melting-freezing point data and multiple arrests (Table 1). Supercooling was common and often severe (as much as 100°C in a few instances), as is illustrated by Fig. 4., which shows a partial cooling curve for $Tl_{1.6}V_{0.4}S_{1.8}$. Here we see arrests reflecting three transitions, the highest of which corresponded to the liquidus surface. The temperature of this surface was not clearly defined by the arrest and therefore was estimated from termination of melting temperatures on the melting point curves, but only to within 5°C. Other compositions along this join gave thermal arrests which were associated with the same transitions but at somewhat different average temperatures. One transition, at approximately 420°C, which was found in most of the runs on the Tl_2S - side of Tl_3VS_4, may indicate a eutectic at about the composition 88 Tl_2S - 12 V_2S_5.

In conjunction with this set of runs, we performed a series of quench-type experiments at selected compositions along this join (Table 2). We observed significant amounts of second and even third phases in all but two compositions, $Tl_{3.01}V_{0.99}S_{3.98}$ and Tl_3VS_4. Polished sections of runs at the three higher temperatures of composition 88 Tl_2S - 12 V_2S_5 showed two phases (Tl_2S + Tl_3VS_4) with eutectic appearance. At lower temperatures, there was no pattern to the intermixing. At compositions between this and Tl_3VS_4, there were two or three compounds which showed no pattern to their intermixing. Sections of runs on the V_2S_5 - rich side were polyphase and often rather blotchy-looking. Pitting was common, and worst in the V_2S_5 - rich materials. The fewest impurities and least amount of pitting were found in compositions Tl_3VS_4 and $Tl_{3.01}V_{0.99}S_{3.98}$, with the latter having a slightly better appearance.

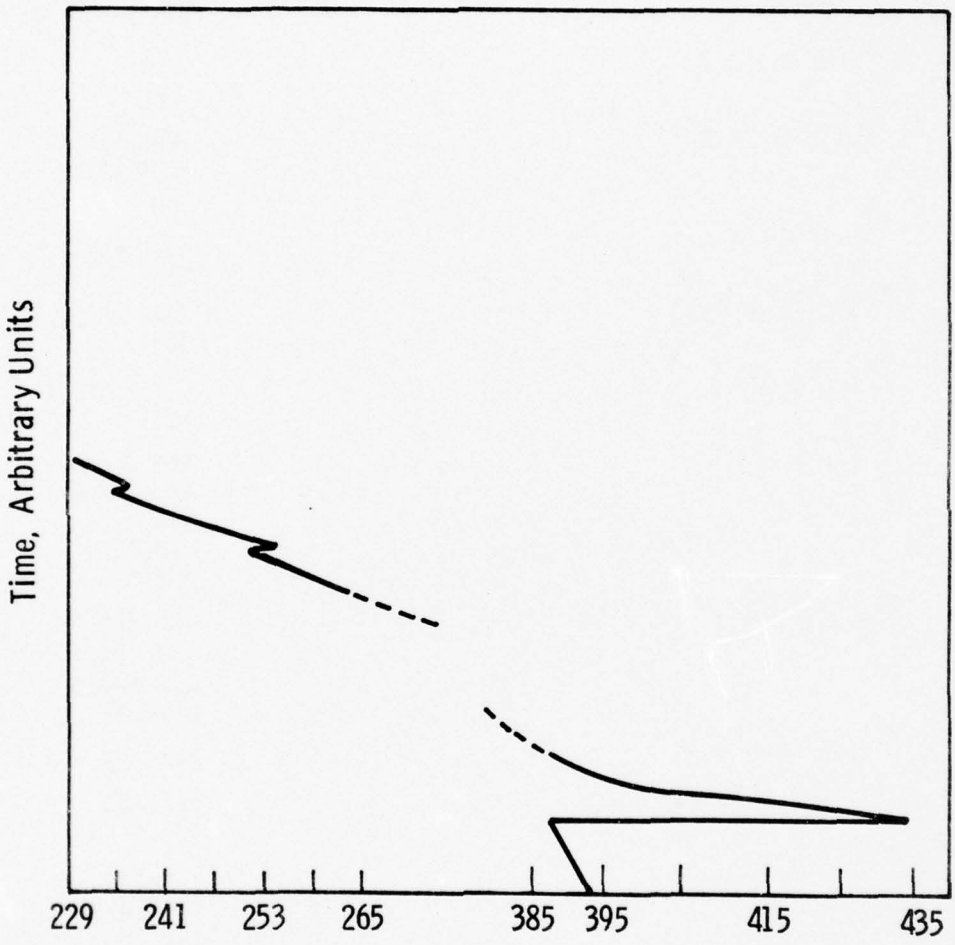

Fig. 4 – Portion of cooling curve for $T\ell_{1.6}V_{.4}S_{1.8}$

Table 1

COMPOSITIONS AND ARRESTS OF THERMAL ANALYSIS RUNS
IN THE SYSTEM Tl-V-S

Composition	*Arrests, T in °C
$Tl_{3.8}V_{0.2}S_{2.4}$	432 411
$Tl_{3.6}V_{0.4}S_{2.8}$	444-446 419-422 414
$Tl_{3.5}V_{0.5}S_{3}$	420-420.5 402
$Tl_{3.45}V_{0.55}S_{3.1}$	418.5-421 391
$Tl_{3.4}V_{0.6}S_{3.2}$	419-423 411.5-413.5
$Tl_{3.3}V_{0.7}S_{3.4}$	506.5-514 450.5-456 444 423-424 253
$Tl_{3.2}V_{0.8}S_{3.6}$	500-505 430-437 254.5-255 233-236
$Tl_{3.08}V_{0.92}S_{3.84}$	522-527
$Tl_{3.04}V_{0.96}S_{3.92}$	521-533 407.5-409
$Tl_{3.01}V_{0.99}S_{3.98}$	524-534 408-409
$Tl_{3}VS_{4}$	522-533 259
$Tl_{2.96}V_{1.04}S_{4.08}$	530-532
$Tl_{2.8}V_{1.2}S_{4.4}$	480.5-490+
$Tl_{2.6}V_{1.4}S_{4.8}$	434.5-445.5+ 418-424 358-367
$Tl_{3}VS_{4.1}$	520-542

Table 1 (Cont.)

COMPOSITIONS AND ARRESTS OF THERMAL ANALYSIS RUNS
IN THE SYSTEM Tl-V-S

Composition	*Arrests, T in °C
$Tl_3VS_{4.04}$	519-541 210
$Tl_{3.2}V_{0.8}S_4$	469-496 240-240.5
$Tl_{3.1}V_{0.9}S_4$	436-451 407-444 219.5
$Tl_{3.04}V_{0.96}S_4$	501-534 350 226.5
$Tl_{3.02}V_{0.98}S_4$	525-534 521-523 373 237
$Tl_{3.01}V_{0.99}S_4$	521-561
$Tl_{2.98}V_{1.02}S_4$	525-539
$Tl_{2.95}V_{1.05}S_4$	524-539+

*In the case of arrests corresponding to the liquidus, the observed extreme supercooling would cause the numbers derived from the cooling curve to be low. The range of temperatures given here are therefore taken from both heating and cooling curves.

+The upper temperatures given here are not those of the highest melting homogeneous melt of this composition. The high-melting compound TlV_5S_8 remained solid throughout the run, so that complete melting did not occur.

Table 2

COMPOSITIONS AND TEMPERATURES USED IN QUENCH-TYPE EXPERIMENTS ALONG THE JOIN Tl_2S-V_2S_5

Tl_2S (mole %)	V_2S_5 (mole %)	T, °C
95	5	552
88	12	240
		402
		508
		530
		552
80	20	240
		402
		508
		530
78	22	240
		402
		530
		552
75.25	24.75	552
75	25	240
		402
		508
		530
		552
72	28	240
		402
		508
		530
		552

Data from the thermal analysis and quench-type experiments indicated that there may be a maximum melting composition at approximately $Tl_{3.01}V_{0.99}S_{3.98}$, but that the join was not pseudobinary. We proceeded therefore to study melting relations along another possible join TlS-VS, and also performed two experiments along the join Tl_3VS_3-S. We hoped the melting point data from the three sets of runs would enable us to map maxima as an aid in finding the maximum melting compositions. The compositions and temperature ranges of arrests are given in Table 1 along with those of previous runs.

Once again, we encountered the problem of poor reproducibility of data, with multiple arrests at varying temperatures and considerable supercooling (as much as 65°C). Doubled freezing-point arrests were encountered in two of the materials ($Tl_{3.01}V_{0.99}S_4$ and $Tl_{3.02}V_{0.98}S_4$), which may have reflected a nearby eutectic or peritectic not on this join, but close to it. We were unable to determine a maximum melting composition from our data, but it appeared to be just on the TlS - rich side of Tl_3VS_4.

Our data from these series of experiments did not permit us to draw conclusions as to the optimum composition for crystal growth. We proceeded to conduct directional solidification experiments, ranging the composition of the charges by small increments around and including the stoichiometric composition. Our silica-glass tube furnaces, initially used for these experiments, proved unsatisfactory for this purpose because of external factors, and the work was transferred to the semi-automated controlled-growth furnace. We were able to run three boules in this setup when equipment malfunction occurred, and we were unable to complete this portion of the work. The three compositions run were $Tl_{3.01}V_{0.99}S_{3.98}$, Tl_3VS_4, and $Tl_{2.99}V_{1.01}S_4$. Portions of the boules were examined using infrared and reflected light microscopy to evaluate their quality. The greatest amount of impurities was found in $Tl_{2.99}V_{1.01}S_4$; the other two boules appeared to contain approximately the same volume of extraneous material. The major impurity in the vanadium-sulphide rich composition was TlV_5S_8. All three boules

Plate 2

72:28 = Tl_2S: V_2S_5

Portion of polished section of quench run at 530°C of composition $Tl_{2.88}V_{1.12}S_{4.24}$ showing two phases Tl_3VS_4 + TlV_5S_8 plus silica.

Magnification = 200 X

contained some silica, but it was in greatest quantity in $Tl_{3.01}V_{0.99}S_{3.98}$, and in fact appeared to be the only impurity in this material.

As part of our study of impurities, we examined some samples of our materials (boules and reactants) using electron probe microanalysis. A conspicuous impurity was silica, and it was found in appreciably greater quantity when the material was either stoichiometric or even more so, rich in the thallium sulphide - rich area of the compositional diagram. When the composition was richer in vanadium sulphide, the proportion of silica to other materials was much less. Here the main extraneous phase proved to be TlV_5S_8, which is a high-temperature melting compound recently reported by Fournes et. al.[4]

We performed additional thermal analysis experiments using the new equipment. Here supercooling was held to a minimum, and we were able to use freezing point arrests only to obtain useful information. Both precision and accuracy were much greater in these runs; the results of some of the runs are given in Table 3. A new set of quench-type experiments also was conducted to help clarify some of the phase relations.

These studies along with some of our earlier experiments, indicate the existance of an extensive field of TlV_5S_8 + Liquid + Vapor on the vanadium - rich side of Tl_3VS_4. This was recognized in polished sections of charges quenched from various V-rich compositions (Plate 2), which showed the presence of a stable solid phase, TlV_5S_8, even at temperatures as high as 900°C.

The occurrence of this compound in phase fields which are in close compositional proximity to Tl_3VS_4 suggests that the composition join Tl_3VS_4 - TlV_5S_8 may act as a pseudobinary join at temperatures near the melting point of Tl_3VS_4. We have not studied compositions on that join. Compositions along the 50 at % S compositional line have, however, been studied and since these lie within = 0.2 at % S of the Tl_3VS_4 - TlV_5S_8 join in the region studied, the data can be

Table 3

COOLING - CURVE DATA IN THE SYSTEM Tl-V-S

*Composition (At. % V)	Arrests, T in°C
12.00	512 ± 2
12.25	518 ± 2
12.50	525.5 ± 1
12.75	525.5 ± 1
13.00	526.0 ± 1

*All runs contained 50 At. % S

applied to indicate the pseudobinary phase relations. Results of appearance-of-phase (quenching) and thermal analysis runs are shown in Fig. 5. Both types of experiments indicate that Tl_3VS_4 may melt incongruently. Thermal analysis data indicates that, if this is so, then the temperature of the invariant reaction $Tl_3VS_4 \rightleftarrows TlV_5S_8+L+V$ is 526 $\pm$ 1°C. The exact composition of the peritectic point was not determined: it must, however, lie at about $Tl_{37.6}V_{12.4}S_{50}$ which is very close to the composition $Tl_{37.5}V_{12.5}S_{50}$ of ideal Tl_3VS_4. At temperatures below the peritectic temperature there are two phase fields present: 1) $Tl_3VS_4+TlV_5S_8+V$ and 2) Tl_3VS_4+L+V. The stability of these fields at temperatures below 500°C was not investigated.

The expected ternary phase relations about the incongruent melting point of a ternary compound are well known and described in standard texts such as that by J. E. Ricci.[5] In the case of Tl_3VS_4, we can show these by using two ternary isothermal sections, one above and one below the invariant point. Above the invariant point (Fig. 6) two phase fields are present: 1) TlV_5S_8+L+V and 2) L+V. The composition Tl_3VS_4 lies within the TlV_5S_8+L+V field. At temperatures below the melting point of Tl_3VS_4, a Tl_3VS_4+L+V field expands into the L+V field and $Tl_3VS_4+TlV_5S_8+L+V$ fields lie on either side of pseudobinary Tl_3VS_4 - TlV_5S_8 join. These will continue to expand with decreasing temperature until other crystallization reactions modify the relations. The expected phase situation at 415°C is shown in Fig. 7.

This interpretation of the phase relations explains why in previous work it was never possible to synthesize a pure Tl_3VS_4 phase by quenching from the melt. There is no composition where a pure phase can be obtained. Moreover, it explains several features of the crystal-growth runs. Inclusions in crystals are always to be expected because of the incongruent nature of the melting relations. Growth rates must be very slow and temperature gradients very steep in order to prevent constitutional supercooling and obtain sizeable lengths of inclusion-free crystal. The growth composition must line on the V-poor

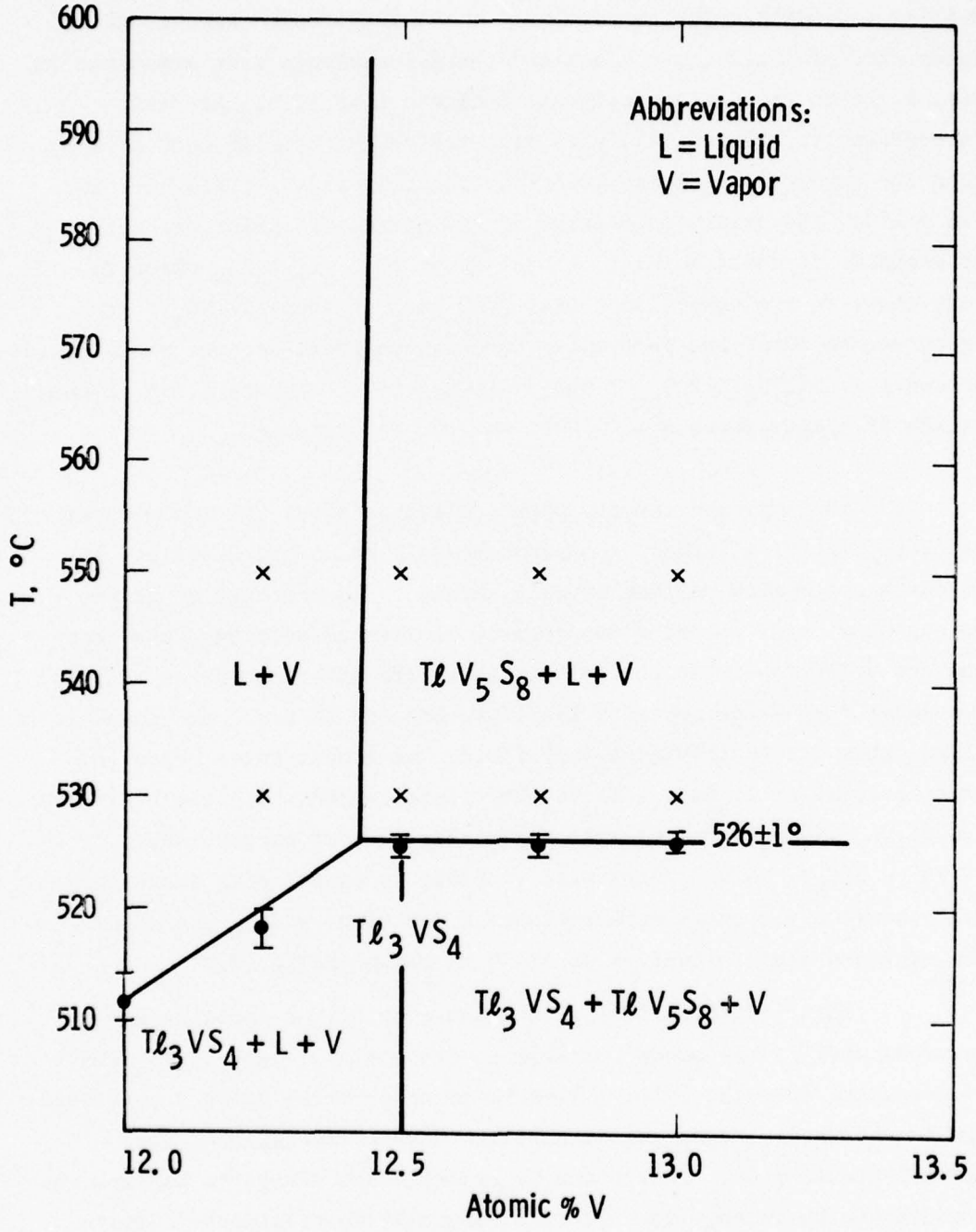

Fig. 5 – A portion of the system Tℓ - V - S along the 50% sulphur line showing phase relations. The crosses represent appearance of phase runs

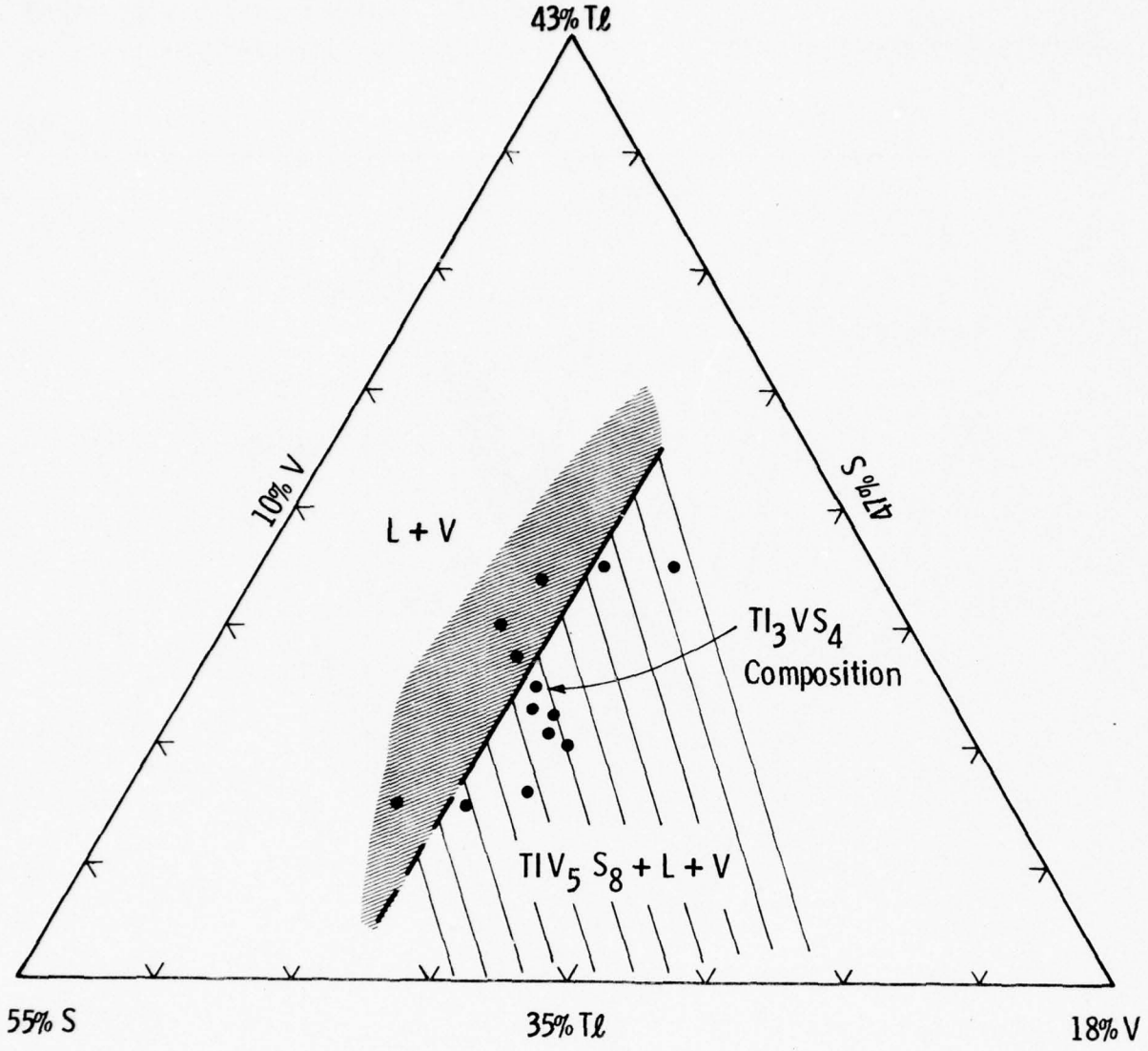

Fig. 6 — A portion of the system Tℓ - V - S at 550°C. The points represent the compositions of appearance - of - phase runs

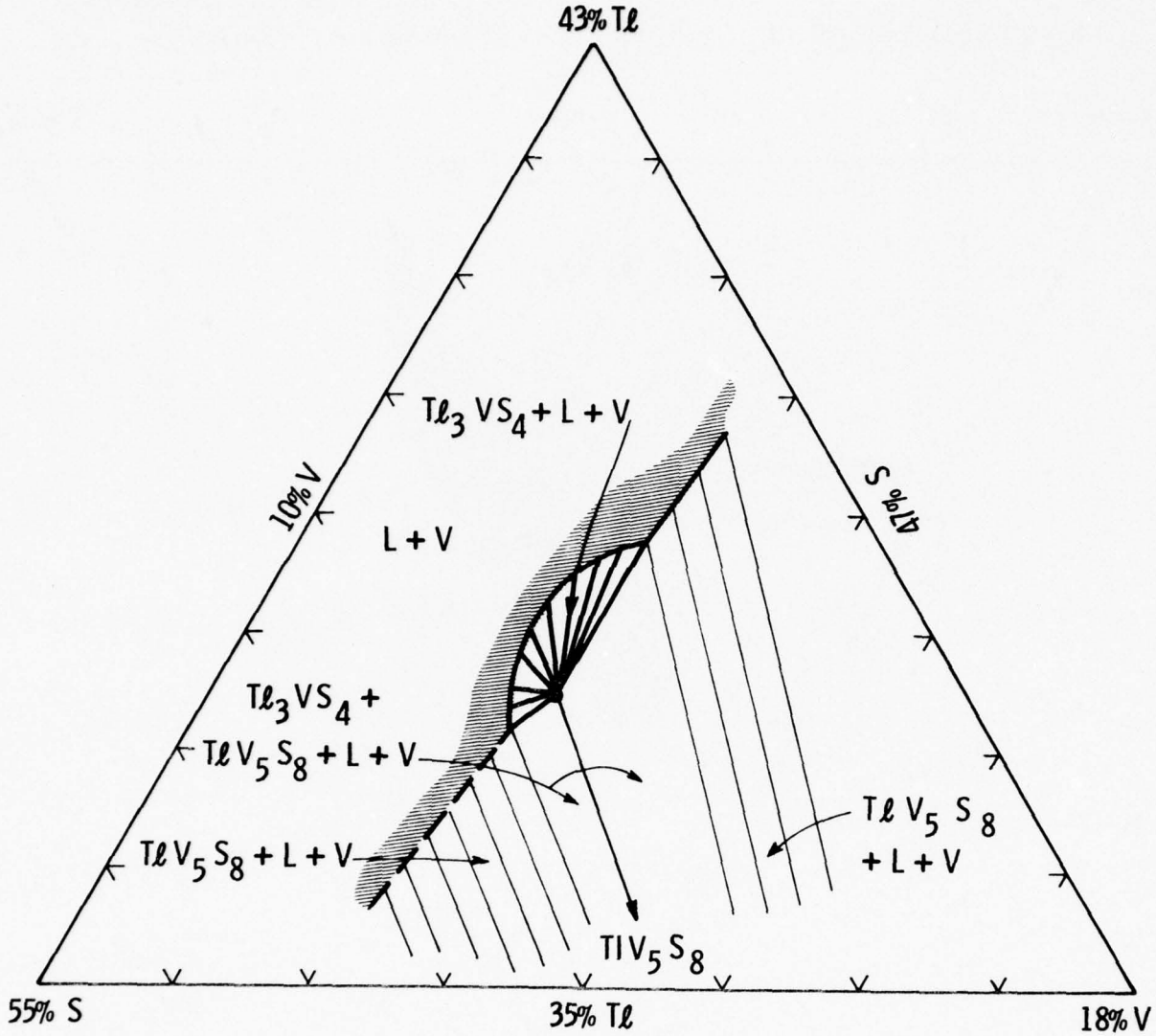

Fig. 7 – A portion of the system Tℓ - V - S at 515°C showing phase relations expected below 526 ± 1°C, the melting point of $Tℓ_3VS_4$

side of the Tl_3VS_4 composition (as found empirically) in that area where Tl_3VS_4 +L+V is the stable phase field. There is no single "best" growth composition as there is for a congruently-melting compound; any composition within the Tl_3VS_4 + L + V field can theoretically give single crystal Tl_3VS_4.

It must be noted that the problems which we encountered in our crystal-growth runs could also be explained by the presence of a eutectic on the join Tl_3VS_4 - TlV_5S_8 close to the composition Tl_3VS_4. In either case, growth of crystals (including composition) would proceed in the same manner.

While this issue is not fully resolved, we have found that we could improve the quality of our crystals by growing from a composition slightly rich in Tl-S as illustrated in Plate 3. Recently we have taken to zone-refining boules by passing reactant contained in an evacuated silica-glass ampoule through the same temperature gradient as that used in growing the crystal, but at a much faster rate (typically 2-3 cm/day). The reactant is removed from the cooled ampoule and the upper portion (usually 3-5 mm thick), containing the bulk of the impurities swept upwards by the refining, is removed. The remaining material is then used to grow crystals as described in Section 2.3. These boules contained fewer impurities than those grown without the intermediate zone-refining step. Crystals grown in the latter part of this study were produced from zone-refined reactants, and all of this work was done in the old-style open furnaces. The crystal used for the filter described on page 48 was grown this way.

Plate 3

Photographs of sections of two crystals illustrating progress in quality improvement studies. The top two photographs are of an early crystal while the bottom are of a recent crystal.

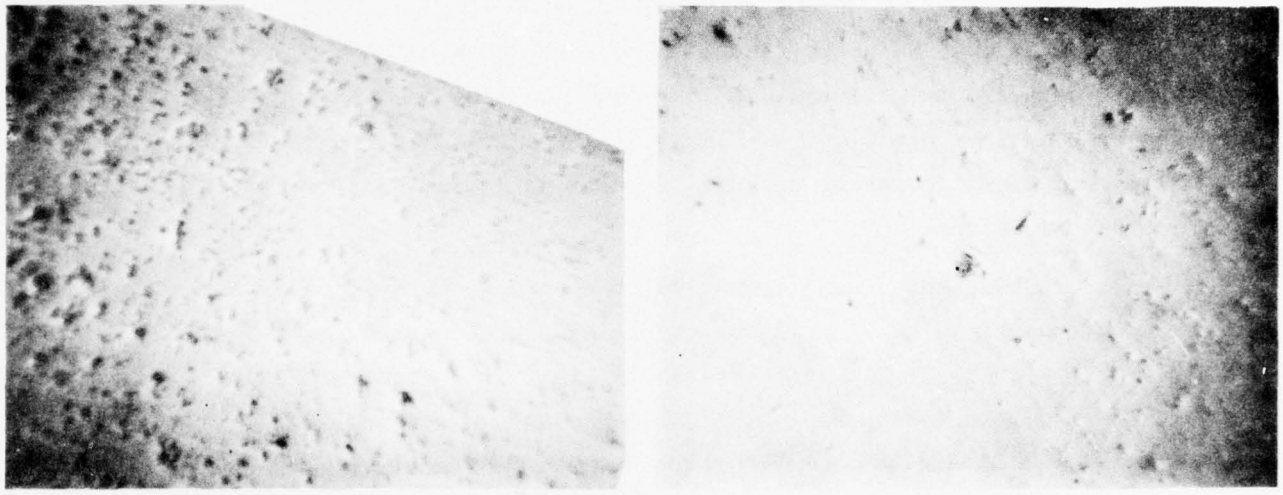

Crystal Number 207057-9

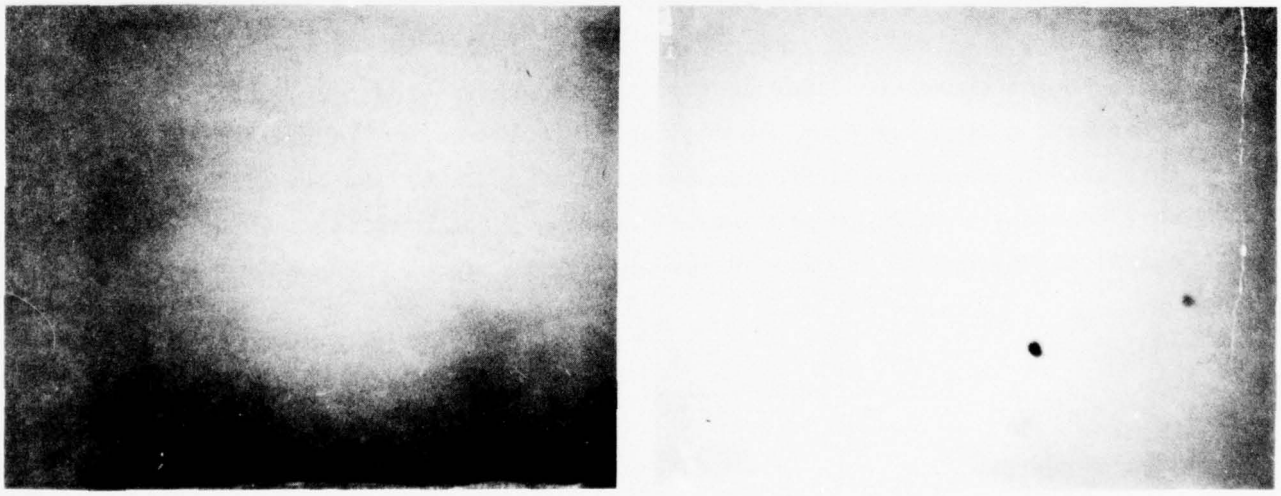

Crystal Number 207057-125

3.3 Study of Crystal Growth Parameters

We have completed two parts of our investigation into the effects of growth parameters on crystal quality. The first was concerned with rate of growth, using rates of 0.94, 1.9, and 4.7 cm/day. The boule grown at the fastest rate was polycrystalline throughout its entire length. The boule grown at the intermediate rate was a single crystal, but it was cracked into several pieces and contained some widely disseminated particles which were clearly visible in reflected light under the microscope. The boule grown at the slow rate was a single crystal and had only a few widely scattered particles which we could see under the microscope in the polished section. There were two cracks in it from hanging up in the growth tube. We found, therefore, that the moderately slow rate of 0.94 cm/day gave the best results. The second part was to ascertain the best gradient at this growth rate, using constant charge composition. Various settings for the two furnaces were used, and the gradients were determined. Figure 8 gives the plots for a number of them. All of the runs to determine the best growth rate were made using a gradient of about 100° per cm (represented by curve c on the figure). In our first run to investigate gradients, we lowered the gradient to about 80°C per cm (curve b). The boule from this run was polycrystalline throughout its length. Apparently, it is necessary to maintain a steep gradient in order to prevent continuous nucleation because of the large amount of undercooling present in this system. The next run was made at a gradient of approximately 115°C per cm (curve d), and the boule was a single crystal. But it contained some widely disseminated fine inclusions. We wanted to further steepen the gradient, but did not wish to do so by raising the temperature in the upper furnace; higher temperatures markedly increase the problem of boule hang up in the tube. We did not wish to further lower the temperature in the bottom furnace as it was at 55% of the melt temperature. The best approach, therefore, was to separate the two furnaces, and several distances between 1/4 and 1 inch were tried and the gradients determined. A separation of 1 inch proved to be too great, producing a depression in the curve (curve f). We found that a separation

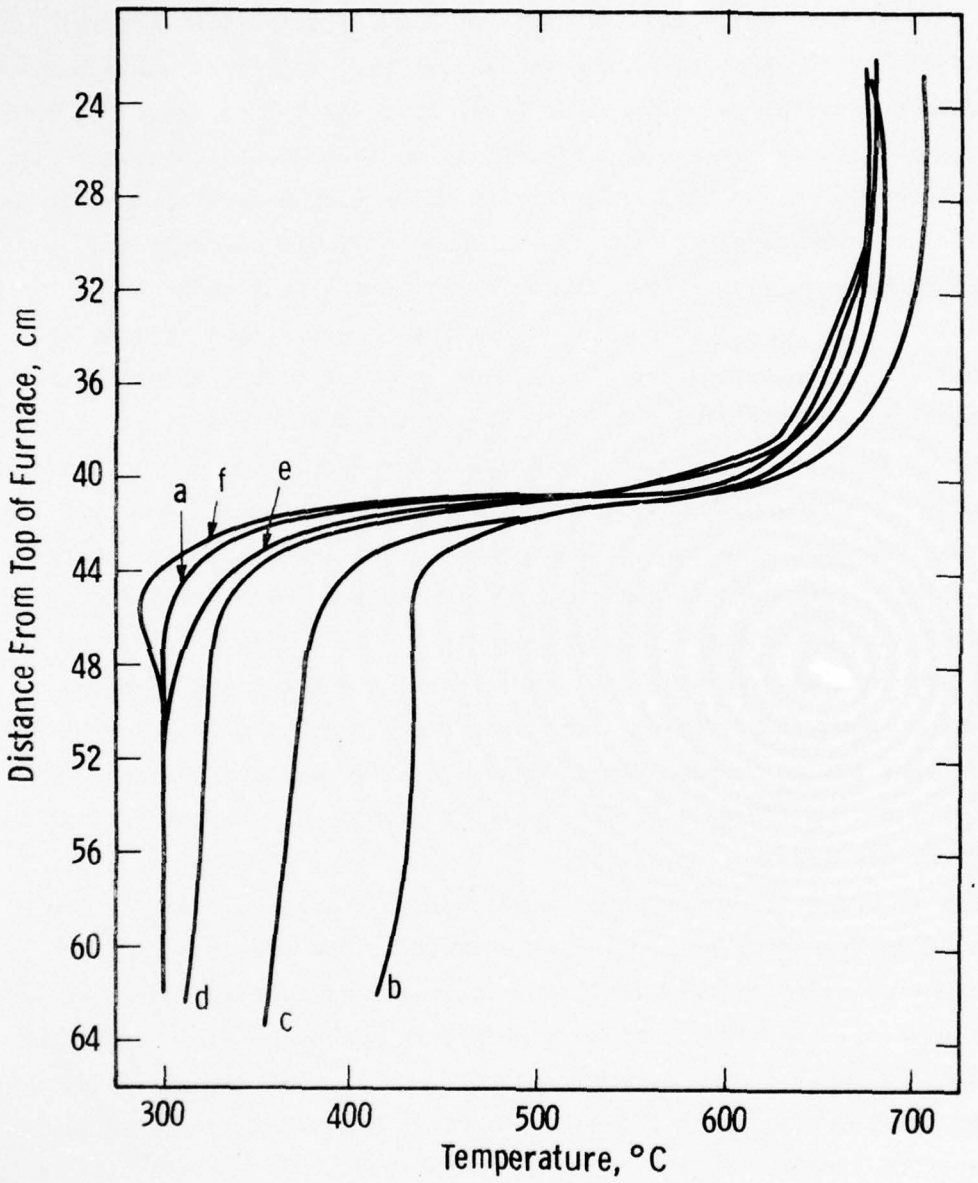

Fig. 8 Temperature profiles of crystal growth furnace at various settings

of 3/4 inch produced the steepest useful gradient, 130°C per cm (curve a). The boule grown at this gradient was the best quality of all those produced in this furnace up to then. It had a 5 cm section of good quality single crystal, of which the central portion of the bottom 4 cm was of high quality (see Section 3.4).

The third part of this study of growth parameters, the effect of various rates of cooling upon crystal quality could not be undertaken during this contract, as we wanted first to complete our work on optimization of composition. We hope to perform this study in the near future.

3.4 The Silica-Glass Container Problem

Early in this study, we noticed hang-up of boules in the quartz-glass crystal-growing tubes, and also what appeared to be reaction of molten material with the ampoule during synthesis of the reactant when the ampoule was held at high temperatures (above 850°C) for periods of more than 8-10 hours. Examination of sections of later grown boules showed that there were considerably more imperfections near the periphery than in the center. While some of this could have been explained by a lateral sweeping of impurities during growth, the presence of silica as an impurity in our materials indicated that there was reaction with the walls of the containers. The severity of the problem was influenced by the type of silica-glass used, being worse when the container was made from synthetic rather than natural quartz. The silica-glass made from synthetic material contains an appreciably higher amount of water than does that made from natural quartz, and it is extremely difficult to remove it. We felt that the water had a deleterious effect on our crystals, at least near the perimeters. But silica-glass is the only suitable container which we have found for this work. To overcome this problem, we tried coating the inside of a tube with graphite, and the results were even worse, as some vanadium carbide was formed and the graphite partially pulled away from the wall of the container. We also considered coating the walls with a noble metal, but preliminary tests showed that our material reacts with these elements; this technique, therefore, could not be used.

In recent months, we have used only silica-glass made from natural quartz, realizing that this step would merely lessen the problem, but not end it. The ampoules still were not water-free, and they had bubbles which could have contained undesirable vapors (water and others) which could migrate under elevated temperatures to interior surfaces. In order to lessen this problem, we used a high-temperature reworking technique to improve the quality of the silica-glass. In this method, the tube is flamed to a white heat using a hydrogen-oxygen torch. The torch is moved

rapidly around the tube to avoid forming hot spots which could distort the cylindrical shape. This treatment tends to collapse near-surface bubbles, to drive off adsorbed water from surfaces, and to polish the interior surfaces. We found that this treatment eased the problem but did not end it. We used it, nevertheless, in all of our later runs. But we do not know of a way to prevent reaction between sample and ampoule.

Parenthetically, the silica-glass container problem is not unique to our family of materials; it also exists for silicon and gallium arsenide, and quartz investigations are being pursued in other laboratories.

3.5 Compounds in the system Tl-Ta-Se

The compositions of compounds in the system Tl-Ta-Se can be described in terms of a phase diagram (Fig. 9) on which known binary and ternary compounds are plotted. There are three compositional phases along the binary Tl-Se, and two along the binary Ta-Se; the compound $TaSe_2$ has four polymorphs. There are two ternary compounds, Tl_3TaSe_4 and $TlTa_3Se_6$.

3.6 Study of Melting Relationships

We made a start on determining melting relations in this system to locate the maximum melting composition for growth of crystals of Tl_3TaSe_4. The technique of thermal analysis (using the large furnaces and ampoules) was used for these initial studies. The experiments involved freezing-melting point determinations along the possible join Tl_2Se - Ta_2Se_5, where Ta_2Se_5 is a hypothetical compound. This join was chosen only to be a starting point for further exploration. In addition to searching for the maximum malting composition, we also were looking for possible eutectics which might affect crystal growth.

A number of runs were made using selected compositions along this join, and the compositions and arrests are given in Table 4; compositions also are shown in Fig. 9 . There was considerable supercooling (as much as 80°C), and some lower temperature arrests, although we did not observe the multiplicity of arrests encountered with Tl_3VS_4. The low-temperature arrest appears to be caused by solidification of Tl_2Se rather than a eutectic. The temperatures of the lower arrests were close to the melting point temperature of Tl_2Se as measured in our apparatus. The maximum melting composition along this join was not located, but it probably is very near the stoichiometric composition. There was too much overlap in freezing-melting point data to be able to pinpoint it. This work was done on the old-style thermal analysis apparatus. We plan to continue the work using the new equipment; the knowledge gained from our most recent studies a Tl_3VS_4 should be of value in selecting data points and interpreting results.

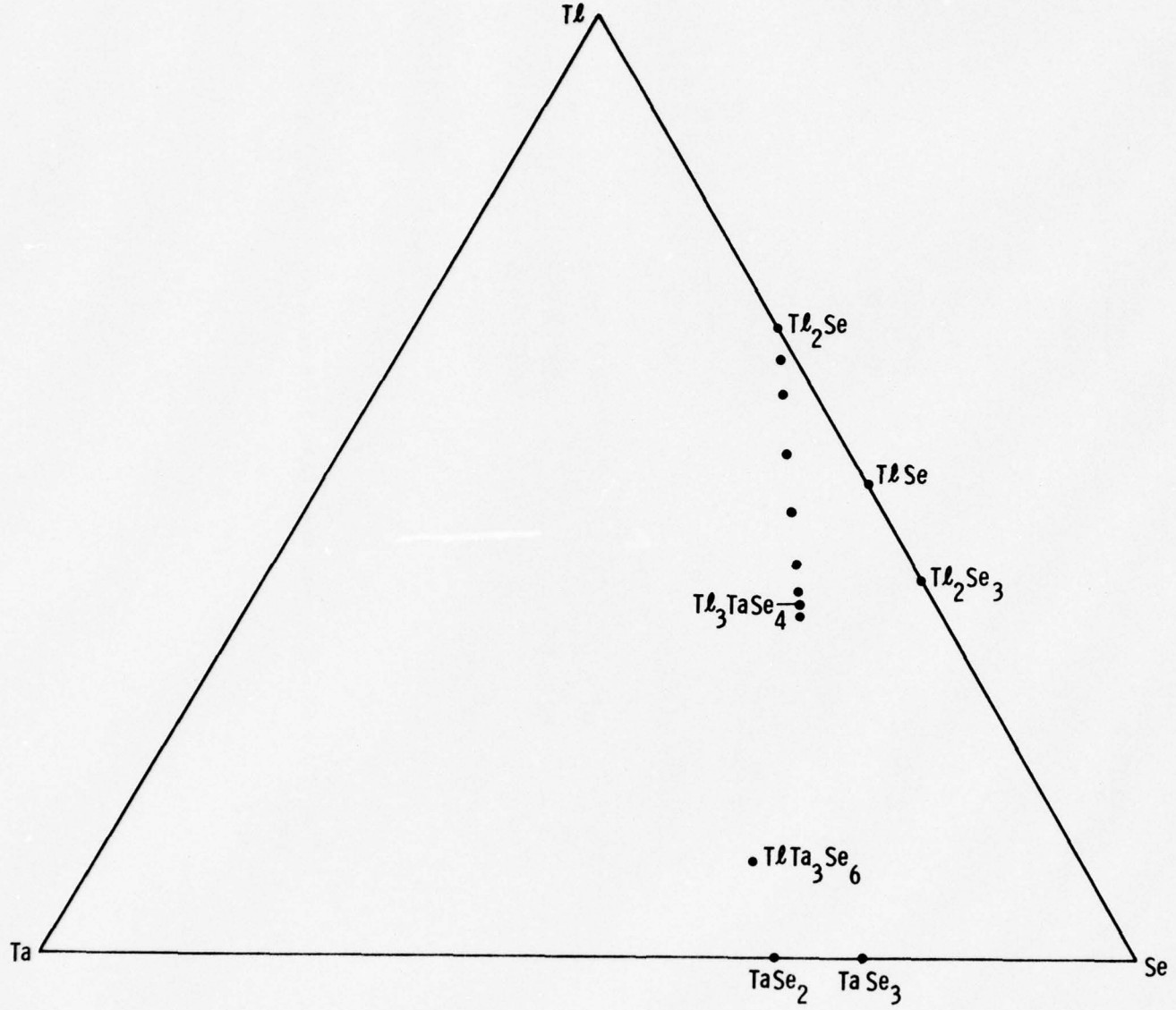

Fig. 9 — The system Tℓ - Ta - Se showing known binary and tenary compounds

Table 4

COMPOSITIONS AND ARRESTS OF THERMAL ANALYSIS RUNS
IN THE SYSTEM Tl-Ta-Se

Composition	*Arrests, T in °C
$Tl_{3.9}Ta_{0.1}Se_{2.2}$	379-381
$Tl_{3.8}Ta_{0.2}Se_{2.4}$	476
	442-450
	375-386
$Tl_{3.6}Ta_{0.4}Se_{2.8}$	518-532
	384-384.5
$Tl_{3.4}Ta_{0.6}Se_{3.2}$	569
	388.5-389.5
$Tl_{3.2}Ta_{0.8}Se_{3.6}$	592-629
	383.5
$Tl_{3.04}Ta_{0.96}Se_{3.92}$	602-635
	383.5
$Tl_{3.02}Ta_{0.98}Se_{3.96}$	632.5-643
$Tl_{3.01}Ta_{0.99}Se_{3.98}$	638.5-643
Tl_3TaSe_4	632.5-643
$Tl_{2.96}Ta_{1.04}Se_{4.08}$	628-639

*The temperature ranges are taken from both heating and cooling curves.

4. STUDY OF ACOUSTIC PROPERTIES

4.1 Overall Objectives

The acoustic work on Tl_3VS_4 comprised two areas of study. The first involved the measurement of material constants such as the elastic, piezoelectric, dielectric constants, the density, and the temperature dependence of these constants. These numbers were then used to calculate surface wave velocities in various cuts and propagation directions as a function of temperature. Orientations were considered useful when the temperature coefficient of delay and power flow angle were small, and the surface wave electro-mechanical coupling factor was large. Interesting directions were then tested experimentally.

The second area of study involved S.A.W. device fabrication and testing on the sulfosalt materials. This work was concerned with techniques of cutting, polishing, and photo lithography, and in general, the surface quality of a finished crystal device. The testing involved measuring insertion loss, frequency response, and temperature stability.

4.2 Material Constants

Tl_3VS_4 has cubic symmetry[6] and therefore has three independent elastic constants, one independent piezoelectric constant, and one independent dielectric constant. The three independent elastic constants C_{11}, C_{12}, and C_{44} were calculated from measured[6] values of bulk wave velocities and densities[6] in conjunction with the following formulas.[7]

For bulk longitudinal waves propagating down the [100]

$$V_L = \left(\frac{C_{11}}{\rho}\right)^{1/2} \qquad (1)$$

For bulk shear waves propagating down the [100]

$$V_S = \left(\frac{C_{44}}{\rho}\right)^{1/2} \qquad (2)$$

For bulk longitudinal waves propagating down the [110]

$$V_L = \left(\frac{C_{11} + C_{12} + 2C_{44}}{2\rho}\right)^{1/2} \qquad (3)$$

and for shear waves propagating down the [110] polarized along the [001]

$$V_S = \left(\frac{C_{44} + e^2/\varepsilon}{\rho}\right)^{1/2} \qquad (4)$$

In the above equations V_L and V_S are longitudinal and shear velocities, ρ is the density, e is the piezoelectric constant and ε is the dielectric constant. Equations (2) and (4) can be used to determine the ratio e^2/ε. Therefore once the dielectric constant has been measured, the piezoelectric constant can be found.

The dielectric constant was calculated from low frequency capacity measurements using a Boonton model 75C capacity bridge. Vapor deposited Cr-Au films were used for the plates and were deposited on (100) faces of Tl_3VS_4. As there is no piezoelectric coupling for the (100) face configuration, the clamped capacity was directly obtained. The measurements were made at 20 KHz on samples which were about 0.1 cm thick.

The bulk velocities used in the above calculations are $V_{[001]} = 2.81 \times 10^3$m/s and $V_{[110]} = 2.46 \times 10^3$m/s for the longitudinal waves, and $V_{[001]} = 0.87 \times 10^3$m/s and $V_{[110]} = 0.96 \times 10^3$m/s for the shear waves. All of the material constants which were measured or calculated from the above formula are shown in Table 5. These values are accurate within a few percent.

TABLE 5 – CONSTANTS OF Tl_3VS_4 AT ROOM TEMPERATURE

Elastic Constants	C_{11}	4.85×10^{10} N/m^2
	C_{12}	1.65
	C_{44}	0.47
Piezoelectric Constant	e_{14}	0.50 c/m^2
Relative Dielectric Constant	$\varepsilon_{11}/\varepsilon_0$	29.0
Density	ρ	6.14×10^3 kg/m^3
First Order Elastic Temp. Coeff.	$\frac{1}{C_{11}} \frac{\partial C_{11}}{\partial T}$	-5.72×10^{-4}/°C
	$\frac{1}{C_{12}} \frac{\partial C_{12}}{\partial T}$	−2.10
	$\frac{1}{C_{44}} \frac{\partial C_{44}}{\partial T}$	0.98
First Order Piezoelectric Temp. Coeff.	$\frac{1}{e_{14}} \frac{\partial e_{14}}{\partial T}$	$\simeq -6.1 \times 10^{-4}$/°C
First Order Dielectric Temp. Coeff.	$\frac{1}{\varepsilon_{11}} \frac{\partial \varepsilon_{11}}{\partial T}$	-0.25×10^{-4}/°C
Thermal Expansion Coeff.	$\frac{1}{l} \frac{\partial l}{\partial T}$	0.25×10^{-4}/°C

4.3 Temperature Coefficients

The temperature variation of the elastic constants was obtained by setting up standing bulk waves in an oriented, cut and polished crystal, and measuring the frequency change necessary to maintain the resonant condition while the temperature was varied. Longitudinal and shear waves were generated with 10 MHz quartz transducers mounted on both ends, and these waves were launched down the [100] and [110] directions. The standing wave resonance will occur at acoustic frequencies which satisfy the relationship.

$$\ell = n\Lambda = \frac{nV}{f} \tag{5}$$

where ℓ is the length of the sample, n is an integer, and Λ, f, and V are the acoustic wavelength, frequency, and velocity.

Differentiating the above expression with respect to temperature yields

$$\frac{1}{f}\frac{\partial f}{\partial T} = \frac{1}{V}\frac{\partial V}{\partial T} - \frac{1}{\ell}\frac{\partial \ell}{\partial T} \tag{6}$$

We can demonstrate from equations (1) through (4) that

$$\frac{1}{V}\frac{\partial V}{\partial T} = \frac{1}{2}\left[\frac{1}{C_e}\frac{\partial C_e}{\partial T} - \frac{1}{\rho}\frac{\partial \rho}{\partial T}\right] \tag{7}$$

where C_e is the effective elastic constant for a particular direction and type of wave. For cubic symmetry,

$$\frac{1}{\rho}\frac{\partial \rho}{\partial T} = -3\frac{1}{\ell}\frac{\partial \ell}{\partial T} \tag{8}$$

where $\frac{1}{\ell}\frac{\partial \ell}{\partial T}$ is the thermal expansion coefficient (which was measured by conventional means). Combining the last three equations, gives

$$\frac{1}{f}\frac{\partial f}{\partial T} = \frac{1}{2}\left[\frac{1}{C_e}\frac{\partial C_e}{\partial T} + \frac{1}{\ell}\frac{\partial \ell}{\partial T}\right] \tag{9}$$

Equation (9) gives the effective elastic constant temperature coefficient in terms of the standing wave frequency temperature coefficient and the thermal expansion coefficient. The plots of standing wave frequency versus temperature were fairly linear over a 45°C temperature range centered about room temperature.

The standing wave frequency method was also used to measure the temperature coefficient of the piezoelectric constant. By comparing the temperature coefficient of frequency for shear waves described by equations (2) and (4), the temperature dependence of the quantity e^2/ε could be determined. The temperature dependence of ε was obtained by performing low frequency capacity measurements as a function of temperature. The above measurements allowed us to calculate the piezoelectric constant temperature coefficient. The temperature coefficients of all the material constants are also included in Table 5.

4.4 Acoustic Attenuation

Bulk attenuation measurements were made on various Tl_3VS_4 samples. The measurements consisted of initiating a pulse (compressional or shear) in a Tl_3VS_4 bulk wave delay line and observing the echo delay on an oscilloscope. We superimposed an exponential trace[8] on the echo pattern to verify that the delay we observed was exponential. We also measured attenuation using a standing wave technique.[9] The two methods agreed to within 20%. The attenuation for compressional waves propagating down the [100] is 0.3db/μs at 30 MHz., and for shear waves propagating down the [110] polarized along the (001), it is 0.9db/μs at 30 MHz.

4.5 Surface Wave Studies

The constants appearing in Table 5 were used to calculate surface wave properties as a function of temperature. We used a modification of a computer program first developed by Campbell and Jones,[10] to calculate surface wave velocity, power flow angle, $^{\Delta V}/V$, and temperature coefficient of delay for surface waves for various cuts and propagation directions in Tl_3VS_4.[11] Similar investigations have been carried out by Jhunjhunwala et. al,[12] and by Henaff and Feldman.[13] These studies have shown that there are a large number of zero temperature coefficient of delay directions. We concentrated on two of the temperature stable cuts of Tl_3VS_4; the (110) rotated cylinder cut found in Ref. (12), and the (001) cut found in our investigations.[14] All of the other known temperature stable directions have significant power flow angles.

The (110) rotated cylinder cuts are specified by the Eulers angles (45.θ.90). For this series of cuts specified by θ, the power flow angle is zero, and for θ = 53° the temperature coefficient of delay is zero. A second zero temperature coefficient was found at 24°.[12] But when the temperature variation of the piezoelectric constant and the dielectric constant were included in the calculation, the 24° direction showed a non-zero temperature coefficient of delay. The 53° angle remained as the only temperature stable direction in the (110) cyclinder cut. Since the theoretical values of velocity, $^{\Delta V}/V$, and temperature coefficient of delay (t.c.d.) are published[12] for the entire range of θ, we will not reproduce the information here. At θ = 53°, the S.A.W. velocity is 1033m/s, $\frac{\Delta V}{V}$ = 0.4%, the t.c.d. is zero, and the power flow angle is zero.

We tested this orientation of Tl_3VS_4 soon after we learned of the zero t.c.d. Before performing experimental verification, we first did our own theoretical calculations and found that when the temperature coefficient of the piezoelectric and dielectric constants were taken into account, the zero t.c.d. occurred at θ = 54°.

At this angle, we calculated the S.A.W. velocity to be 1023 m/s, and we measured the velocity to be 1015 m/s. This is considered to be good agreement as it is difficult to orient the sample and align the I.D. grids to better than 1/2 degree. We also measured k^2 to be 0.6% compared to the theoretical value of 0.8%. The crystal used for these studies was of composition $Tl_{3.01}V_{0.99}S_{3.98}$ and was cut to a size of approximately 1 cm square and $\sim$ 0.2 cm thick.

A pair of I.D. grids were put down on the polished surface, the bottom surface was fine ground, and a comparison was made of the phase of a signal going through the device with that of a reference signal, while varying the temperature of the crystal. The phase difference was kept constant by varying the frequency of the signal. The crystal orientation and the results of this study are shown in Fig. (10). We found a temperature stable region from 30° to 80°C, within which the fractional change in delay time was $\pm$ 50ppm. This figure translates into a temperature coefficient of delay of $\pm$ 1ppm/°C.

We also measured insertion loss on this device and found an unusually large value of about 90db. Since the experiments were done at 10 MHz, we expected little surface wave attenuation between the grids which had a separation of 0.6cm. Also, the measured effective value of $\sim$0.6% for each I.D. grid was inconsistant with this high loss. We felt therefore that this propagation direction may lead to "leaky" surface waves or bulk wave generators. We then accelerated our work concerning the modification of our computer program to account for leaky waves. These modifications will be discussed in a later section. Our conclusion at this time concerning the 110 rotated cylinder cut is that the surface wave probably is not leaky and we must find another explanation for the insertion loss. It is possible that micro cracks which we could not detect by visual inspection were responsible for it. Since this cut has many desirable properties for device application, we intend to conduct additional studies on the problem of high insertion loss.

One of the first directions found having a zero power flow angle and a small t.c.d. was the (001) cut, [100] propagating.[14] The results of our initial computer study for the (001) cut of Tl_3VS_4 are shown in Fig. 10. The theoretical curve for the t.c.d. shows a zero for surface waves propagating at nearly 30° away from the [100]. However, the power flow angle for this direction is ∿9 degrees. For surface waves propagating along the [110], the power flow angle is zero, and the effective surface wave coupling factor k^2=1.4% is at its maximum value for this cut. The t.c.d. for the [110] propagation direction is not zero but has a small positive value of ∿15ppm/°C.[14] This direction is not leaky and is considered useful for device applications.

We fabricated and tested a S.A.W. filter on the [110] propagating, (001) surface of Tl_3VS_4. The passband filter had a bandwidth of 3 MHz, and was centered at ∿23.5 MHz. This filter is described in detail elsewhere.[14] We encountered a fairly serious problem with it; the insertion loss of this filter at mid band was 45db which is much higher than was expected for this material. This led to an investigation of the surface quality of the crystals used for the filter, which is discussed in section 4.6.

A second series of low frequency S.A.W. filters was fabricated[15] using polishing procedures developed by this study.

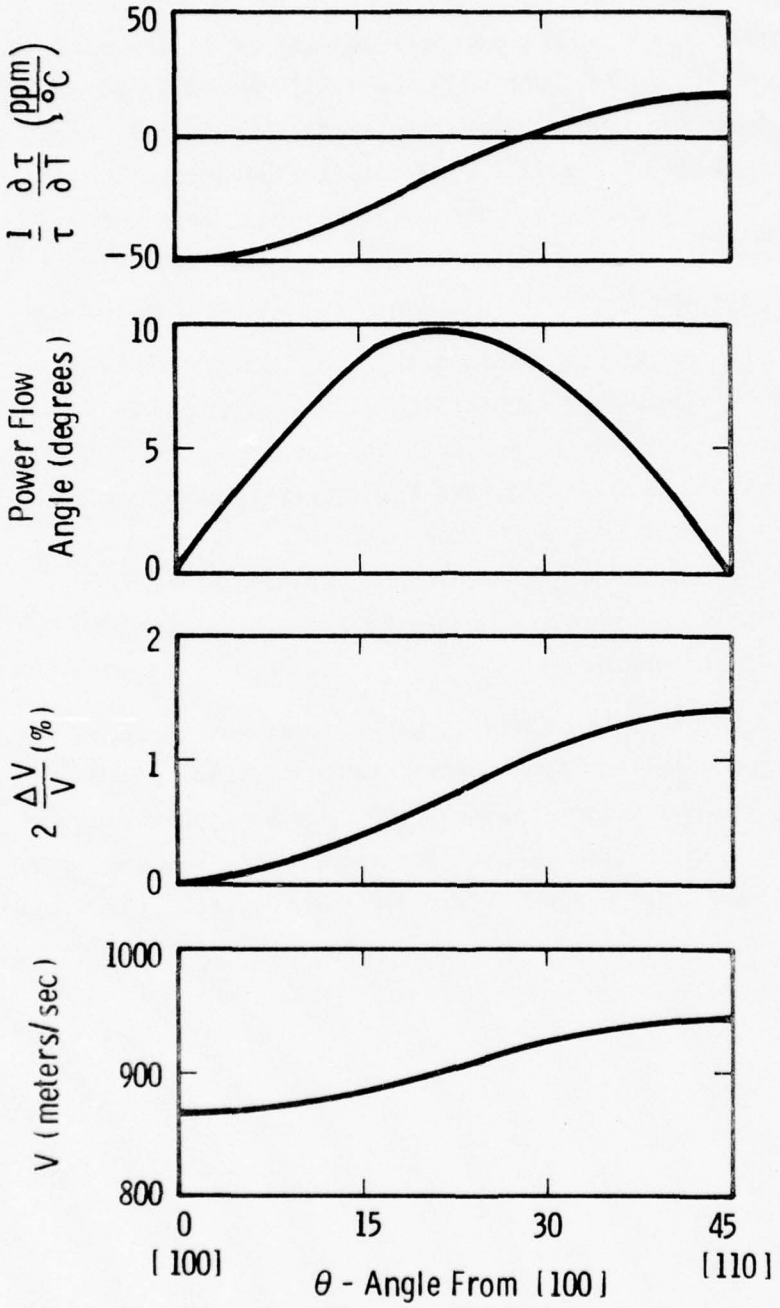

Fig. 10 – Surface wave velocity, $2\frac{\Delta V}{V}$, power flow angle, and temp. coeff. of delay for propagation on the (001) plane of Tl_3VS_4

A filter with a normal center frequency of 70 MHz on a quartz substrate (Fig. 11), was fabricated on the (001) cut of Tl_3VS_4. With the filter oriented for [110] propagating surface waves, the center frequency of the Tl_3VS_4 filter was 21.3 MHz, the bandwidth was $\sim$ 1.1 MHz and the insertion loss was 30db. The third harmonic response was centered at 64 MHz, with a bandwidth of $\sim$ 1.2 MHz and an insertion loss of 25db. These responses for the Tl_3VS_4 filter are shown in Figures 12a and 12b.

Both the fundamental and the third harmonic responses for the Tl_3VS_4 filter give reasonable replication of the quartz filter response, and the third harmonic leads to a 10db lower insertion loss than the quartz filter. The insertion loss for this sulfo-salt filter is better than that of our first device by $\sim$ 15db, and this improvement is the result of better surface quality. The interference on the high frequency side of the passband is caused by bulk waves[14]; these effects will be discussed elsewhere.[15]

In fabricating this filter, our interest was in comparing Tl_3VS_4 with quartz (the only temperature stable material presently being used) for general filter applications. We have therefore not included a discussion of its design. The results clearly demononstrate that Tl_3VS_4 has excellent potential for devices requiring low frequencies (under 100 MHz).

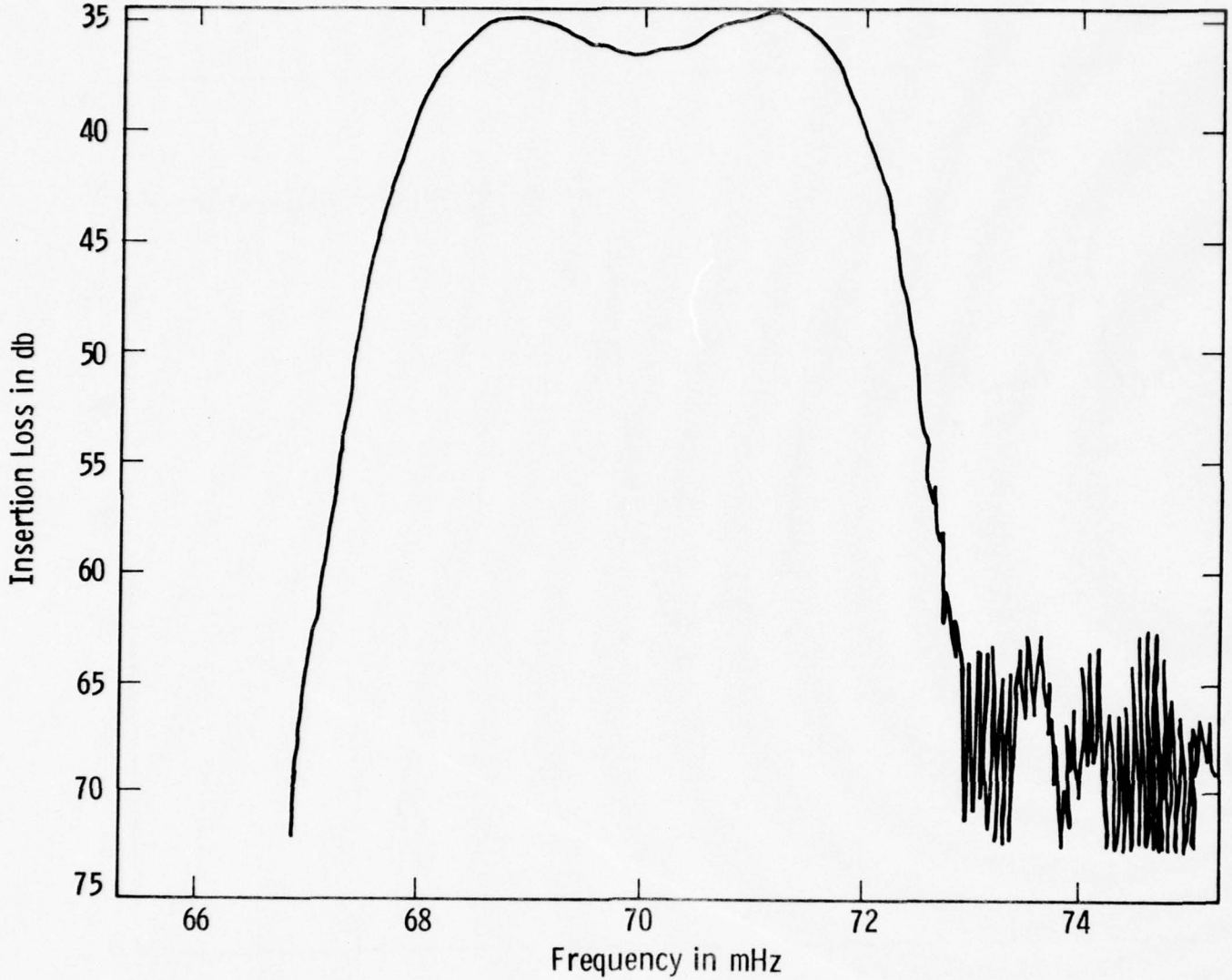

Fig. 11 – S.A.W. filter response ST cut quartz

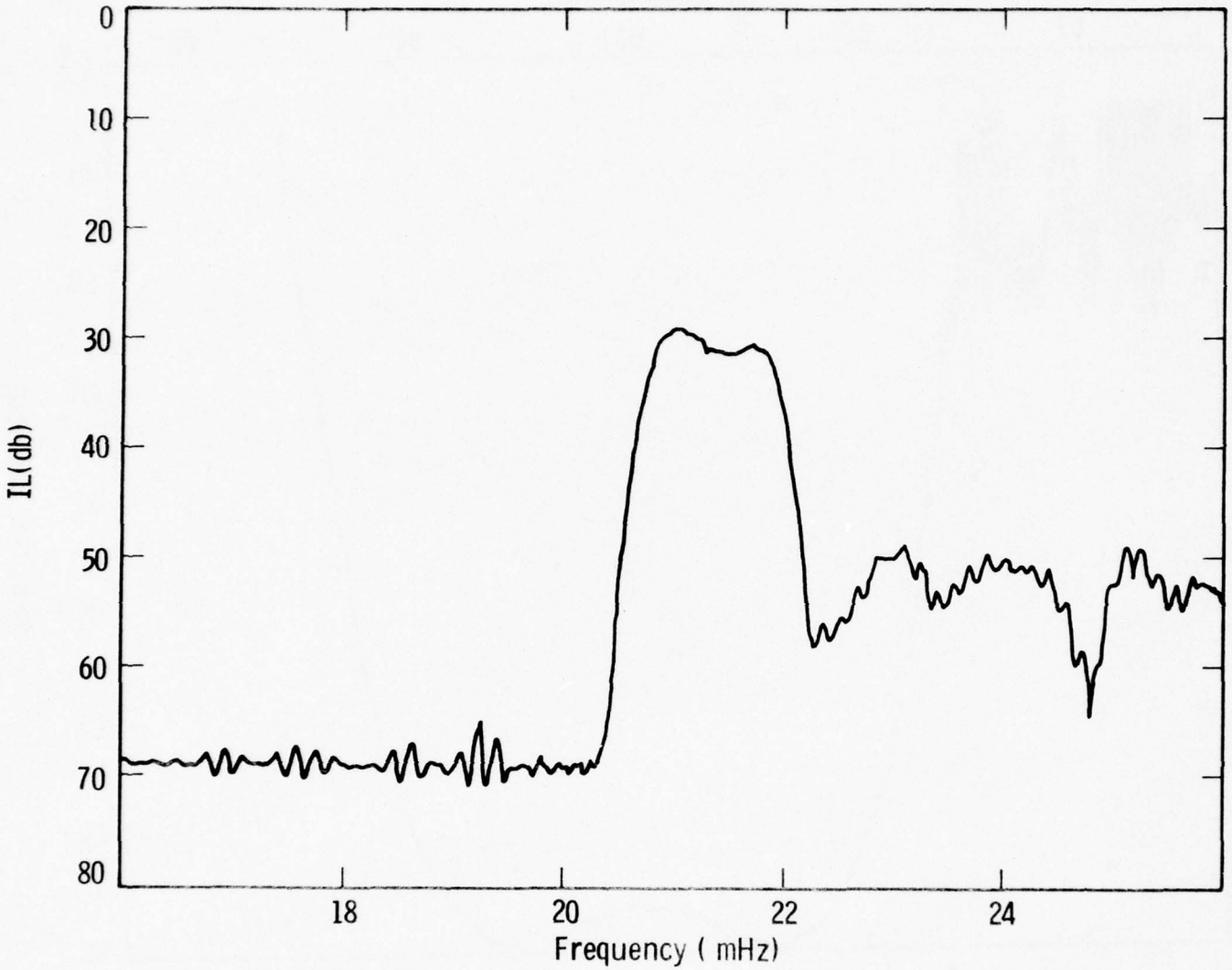

Fig. 12a – S. A. W. filter response (001) cut of Tl_3VS_4 (Fundamental)

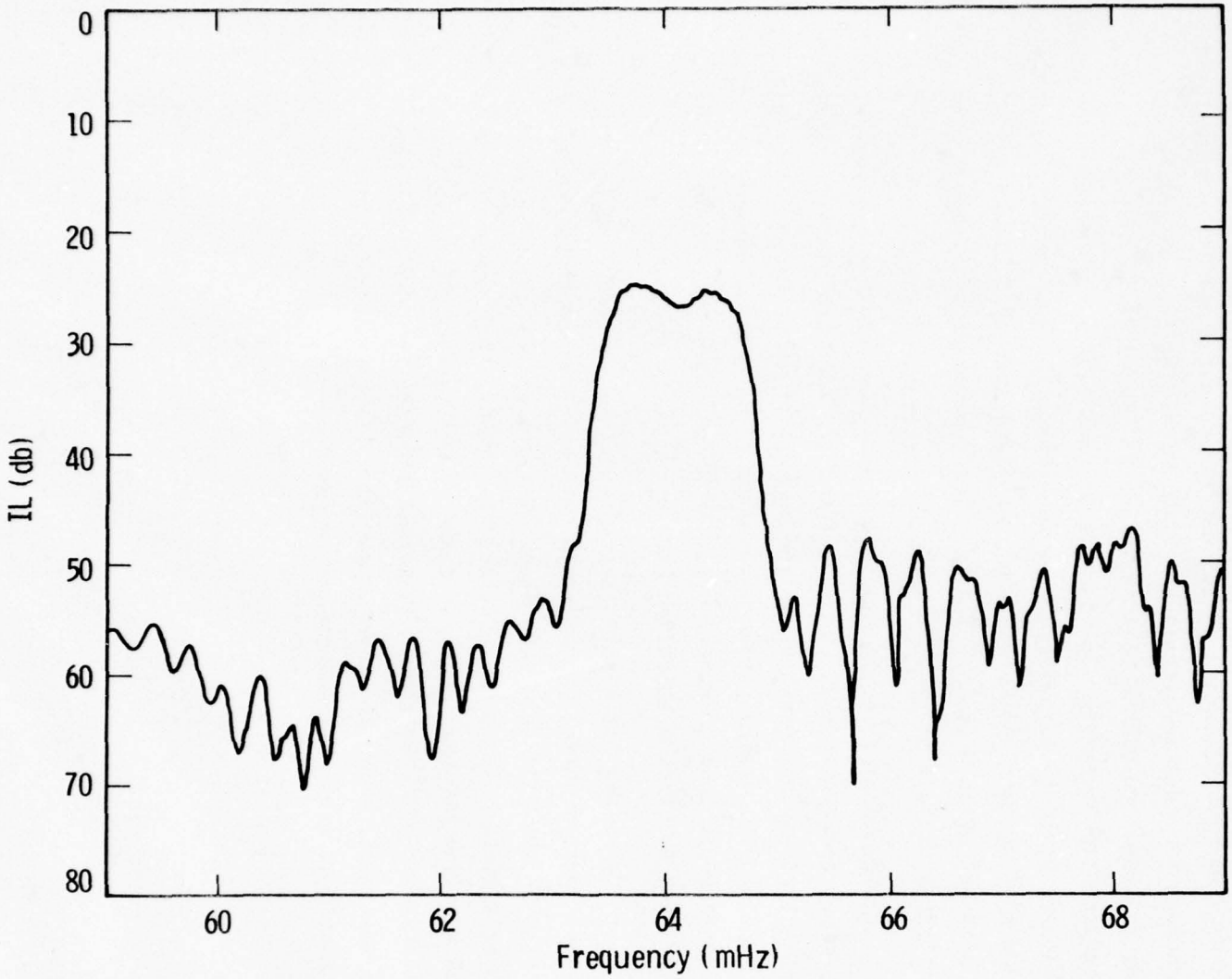

Fig. 12b – S.A.W. filter response (001) cut of Tl_3VS_4 (3rd Harmonic)

4.6 Study of Surface Effects of Cutting and Polishing

We have investigated the nature and extent of the damage layer remaining on oriented crystals of Tl_3VS_4 after cutting and polishing. X-ray and electron diffraction techniques were used in this study. Since a chemical etch suitable for removing surface layers has not been developed, etching was performed using a Veeco ion beam milling system. With a milling current of $0.8mA/cm^2$, anode voltage of 1 kV and a bell jar pressure (with argon) of 2×10^{-4} Torr, material was removed from the crystal surface at a rate of $\sim$8-9μ/hr.

The first crystals examined showed that visible evidence of mechanical damage was still present after 12μ had been removed. Most scratch traces disappeared after the removal of about 24μ. The original polished and the milled surfaces were examined. Evidence based on Weissenberg and Laue diffraction patterns indicated that an amorphous region over 20 microns thick had been produced by polishing.

We worked out a polishing procedure which improved the surfaces considerably. The crystals were polished in steps, changing the size of the grit with each step down to a grit size of 0.1μ. At each grit size, a layer of material was removed which was at least as thick as twice the previous grit diameter. After the final polish with the 0.1μ grit, we found the damage layer to be less than 0.2μ. With this small a damaged layer, the ion milling step could be eliminated at least for low-frequency devices.

5. HALL MEASUREMENTS

Van der Pauw Hall Samples were examined in an effort to determine net carrier densities, conductivity and mobility. Preliminary measurements failed at resolving any of the above parameters. The material displayed a relaxing current voltage behavior which prohibited resolution of the small voltages necessary for a meaningful measurement. This behavior is reminiscent of relatively slow traps (30 seconds and larger). Additionally, we had reason to be suspicious of the ohmic contacts used for the Hall Measurement. As viewed with a DC ohmmeter, the material appeared to have a somewhat variable impedance. In an effort to determine whether this could be attributed to a bulk or contact effect, a comparison sample was fabricated by heating the substrate during the deposition cycle in the evaporator. Unfortunately, this attempt gave a very high impedance reading on the ohmmeter. It appears that a somewhat broader investigation is in order to insure reasonable contacts which will not become part of any Hall measurement problem. This would entail a systematic investigation of several metals and a variety of deposition conditions on similar pieces of Tl_3VS_4 to try and minimize the apparent device impedance. With this situation well in hand, it would then be more appropriate to perform the Hall Measurements to determine the origin of the initial anomalous results.

6. COMPUTER PROGRAM†

The computer program originally developed by Campbell and Jones[10] has been the principle analytical tool for analyzing the surface wave properties of piezoelectric crystals. Because of the design of the program, the only acceptible solutions are those that occur for surface wave velocities lying below that of the lowest bulk wave. These are the true surface waves, and the boundary conditions require that they be composed of a superposition of the four solutions to the equations of motion that have exponentially decaying amplitudes in the crystal bulk.

The program is capable of scanning over a range of propagation directions that may include those for which the surface wave velocity would be greater than that of the lowest bulk wave. As the lowest bulk wave velocity is approached, the boundary condition determinant cannot be satisfied. The program was not able to treat this situation adequately and gave little or no useful information.

In a previous report we indicated our intention to generate a map of the minimum value of magnitude of the boundary condition determinant. This was to be used as a guide to the user to enable him to recognize patterns in this function that would point out regions of leakiness of the surface waves. In the course of implementing this approach, we felt that there may be some usefulness to leaky waves and, rather than throwing away the information about them, the program should be modified to handle them and to provide information about their acoustic properties.

The approached to leaky waves is to allow the velocity of propagation to be complex. Hanebrekke[16] discusses the procedure for selecting which four of the eight possible roots to the secular equation derived from the equations of motion are the correct ones to use in

† The computer program has been developed with Westinghouse funds.

fitting the boundary conditions when the velocity is complex. The solution in this case is called a "leaky wave" to denote a wave in which the energy is not confined to the surface, but leaks into the bulk.

Whereas the normal surface waves utilize four waves decaying into bulk, leaky waves make use of one component that actually grows in the direction of the bulk. This does not imply infinite amplitude at infinity, only that the amplitude of the wave grows relative to that at the surface.

The modifications to the program have been made; however we have just discovered a defect in our implementation which is the algorithm for selection of the proper set of roots to send to the boundary conditions. This is currently being fixed.

Since leaky waves require a search in two dimensions (the real and the imaginary parts of the complex velocity), the existing one dimensional search algorithm had to be replaced. The algorithm chosen to find the solution was a modified version of PATTRNSEARCH, a multidimensional minimization routine developed by Hooke and Jeeves.[17]

After considerable experimentation, it was decided that PATTRNSEARCH requires so many calls on the function to be minimized that the cost of running the program becomes excessive (e.g. to find the velocity for a single propagation direction for both the metallized and free surfaces requires almost a minute).

We have conceived of an alternate procedure for finding the complex velocity at which the boundary conditions will be satisfied. It makes use of the fact that the boundary condition determinant is an analytic function of the complex velocity since it is in fact a polynomial in v^2.

By using the Cauchy integral relation

$$f(Z_o) = \oint \frac{f(Z)}{(Z-Zo)}\, DZ \qquad (3)$$

where f(Z) represents the determinant in question, we can avoid running through the main program while running the search, and instead evaluate the function on the boundary of a rectangular contour surrounding the solution. Equation (3) states that the value of the function at Zo is determined entirely by the value of the function on the boundary. This procedure will allow us to actually run through the time consuming portion of the program only a relatively small number of times (approximately 25 points on the boundary). The search for the zero in the determinant would be performed on the integral given by (3) using the tabulated values of f(Z) on the boundary (a fixed set for each direction of propagation) and adjusting Zo = Xo + iYo.

The computer program has been much improved; the remaining bugs appear to be minor and are expected to be cleared up shortly. The modifications in the search function described above are expected to improve the speed by an order of magnitude, allowing studies of surface waves to extend into the leaky wave region.

ACKNOWLEDGMENTS

We wish to thank Dr. M. H. Francombe for studies of surface damage, and W. E. Gaida, C. Chamberlain, D. H. Watt and R. Storrick for technical assistance. The Hall measurements were performed by Dr. D. Barrett and V. Wrick. R. A. Moore, F. Halgas, and R. Sundelin fabricated the SAW device and performed the measurements on it. Dr. G. W. Roland assisted in phase diagram study. R. Palmquist performed the electron probe microanalysis.

REFERENCES

1. A. Wachtel, A New Furnace and Technique for Melting-Point Determinations of Sulfosalt Materials. (To be Published)
2. G. W. Roland, J. P. McHugh, and J. D. Feichtner, Jour. Electronic Mat. 3, 829 (1974).
3. G. W. Roland, J. D. Feichtner, M. Rubenstein, and W. E. Kramer, Final Technical Report for ARPA Contract F33615-72-C-1976, AFML-TR-76-173 (1975).
4. L. Fournès, M. Vlasse and M. Saux, Mat. Res. Bull., 12, 1 (1977).
5. J. E. Ricci, The Phase Rule and Heterogeneous Equilibrium. D. Van Nostrand, New York, 505p. (1951).
6. T. J. Isaacs, M. Gottlieb, M. R. Daniel and J. D. Feichtner, J. Electronic Mat., 4, 67 (1975).
7. J. de Klerk, Rev. Sci. Inst., 36, 1540 (1965).
8. J. de Klerk, Ultrasonics, 2, 137 (1964).
9. D. I. Bolef and J. de Klerk, IEEE Trans. Ultrasonics Eng., UE-10, 19 (1963).
10. J. J. Campbell and W. R. Jones, IEEE Trans. Sonics Ultrasonics, SU-15, 209 (1968).
11. R. W. Weinert and T. J. Isaacs, Proc. 29th Ann. Freq. Control Symp., 139 (1975).
12. A. Jhunjhunwala, J. F. Vetelino and J. C. Field, Electronics Lett., 12, 683, (1976).

13. J. Haneff and M. Feldmann, Electronics Lett., 13, 300 (1977).

14. R. W. Weinert, T. J. Isaacs, F. Halgas, J. T. Godfrey and R. A. Moore, Ultrasonics Symp. Proc., 532 (1976).

15. F. Halgas, J. Godfrey, R. Sundelin, R. A. Moore, R. W. Weinert and T. J. Isaacs, Ultrasonics Symp., Proc., (1977). (to be published).

16. H. Hanebrekke, Norwegian Tech. Inst. ELAB Rept. TE 173.

17. R. Hooke and T. A. Jeeves, Jour. A.C.M., 8, 212 (1961).

APPENDIX

"A New Furnace and Technique for Melting Point Determinations of Sulfosalt Materials," by A. Wachtel, Westinghouse Report 77-1C4-CGROW-R1.

The work described in this report was performed using Westinghouse internal funding only, and was part of an ongoing project on crystal growth studies.

A NEW FURNACE AND TECHNIQUE FOR MELTING POINT DETERMINATIONS OF SULFOSALT MATERIALS

A. Wachtel
Westinghouse Research & Development Center
Pittsburgh, Pennsylvania 15235

ABSTRACT

A light furnace with low thermal mass is described which permits the determination of thermal arrests of less than 1 mℓ of substance sealed in ampoules which contain a side arm with seed material. Seeding is easily accomplished by tilting the entire furnace by hand. Seeding eliminates low values for melting points in systems showing severe supercooling. Other advantages of the present equipment include speed and reliability due to the absence of thermal and compositional inhomogeneities which are inherent in large charges.

A NEW FURNACE AND TECHNIQUE FOR MELTING POINT DETERMINATIONS OF SULFOSALT MATERIALS

A. Wachtel
Westinghouse Research & Development Center
Pittsburgh, Pennsylvania 15235

1. INTRODUCTION

Considerable effort has been applied in recent years, both at the Westinghouse R&D Center and elsewhere, to the crystal growth and characterization of sulfide and sulfosalt material. This work began in about 1969 with the growth of crystals of proustite (Ag_3AsS_3) and pyrargyrite (Ag_3SbS_3). Since that time, Tl_3AsSe_3 (TAS) and various Tl-As-P-S-Se compounds became of considerable interest for nonlinear optical processing and other studies and, more recently, compounds in the Tl-Ta-V-S-Se system showed promise for both bulk and surface wave acoustic devices. These ternary compounds are in chemical systems which have complex melting relations. It has been found (e.g., see Ref. 1) that considerable attention must be paid to identifying the exact congruently-melting composition for each compound (nonstoichiometry is often involved) and achieving that composition reproducibly in crystal growth experiments. Otherwise, the crystals invariably contain second-phase inclusions and their usefulness as optical or microwave materials is usually severely degraded. A large amount of time has, therefore,

been devoted to phase diagram studies and melting-point determinations in various sulfide- and selenide-containing systems in order to determine maximum melting compositions which are the only ones to crystallize in a single phase.

2. DISCUSSION OF THERMAL ANALYSIS

In the usual methods of determining the temperature of phase changes in chemically inert substances (e.g., by DTA), considerable accuracy is achieved by immersing the thermocouple directly into the sample. This can be accomplished despite the fact that a very small sample ($\sim$0.1g) is confined in a well bored in a massive block of Pt which constitutes an effective heat sink to ensure that, except during phase changes, the sample temperature equals that of the reference substance (Al_2O_3) in an adjacent well. An occurring phase change is signaled by a differential temperature between the two thermocouples because of heat of reaction absorbed or evolved. Another arrangement frequently employed generates simply a heating or cooling curve by measuring the sample temperature only. Reactions which occur in a single-phase sample are reflected as plateaus on the temperature-time curve (dT/dt) because these are invariant (T-constant) in a thermodynamic sense. These latter curves are frequently more sensitive for melting point determinations because no extrapolations of beginning or ending of melting are necessary as in the DTA type of experiment.

At elevated temperatures, the sulfosalts under present investigation (Tl_3AsSe_3, Tl_3VS_4, $CuSbS_2$, etc.) pose special problems which make it impossible to achieve heat transfer by conduction via physical contact with the thermocouple:

1. Appreciable vapor pressure of more volatile components (e.g., S).

2. Reactivity with O_2.

3. Reactivity with metallic containers and thermocouple materials.

This means that the sample must be sealed under vacuum or an inert gas. The lack of direct physical contact between sample and thermocouple opens competing pathways for heat transfer, e.g., heat conducted through the leads of the thermocouple or radiation from the furnace wall below the ampoule reflected into the well of the ampoule. In order to minimize these competing effects and to ensure that the thermocouple responds mostly to the temperature of the sample, it follows that the ratio of thermal mass of the furnace compared to that of the sample should be as small as possible. Previously,[1] this was accomplished by the use of large (∿40g) samples in ampoules with deep wells. The present object was to reduce sample size to 0.7-0.8 mℓ (∿5.5g for TAS) which is sufficient to cover the top of the 10 cm high, 4 mm O.D. well inside a 10 mm I.D. ampoule.

The primary advantage of smaller sample size lies in the more easily-obtainable compositional uniformity compared to large samples. Reaction times for reactant preparation of a few days can suffice compared to weeks for samples 50g or more in weight. Also, thermal homogeneity is achieved at a faster rate so that excessively slow heating and cooling rates are unnecessary. Associated with this is the possible reduction of a hypothetical source of error: slow cooling of a large volume of

melt may cause the segregation of minor phases in a portion of the ampoule which is remote from the thermocouple. Especially with more rapid cooling the effect of differences in stoichiometry may then be reduced. Another advantage is that less material need be synthesized. This not only saves time, but also diminishes the likelihood of explosions and their seriousness if one should occur.

A major problem in the thermal analysis of sulfide-type materials is caused by the propensity of the melts to supercool, often by as much as 10°-30°C, and occasionally up to 100°C or more. The consequences of this are shown in Fig. 1, which compares an ideal heating-cooling curve with one obtained when supercooling prevails. The result is that true melting points are not obtained on cooling. Because of heat transfer kinetics, heating arrests (points 1 to 2) are, in practice, somewhat higher than the true melting points and also continue to slope upwards. Cooling arrests are normally flatter, but may also slope downwards if, at the onset of freezing (point 3), the furnace temperature drops too rapidly. In either case (low or rapidly dropping furnace temperatures) the data are inadequate for precise compositional determinations of the location of maximum-melting compounds. The system to be described allows for the seeding of the melt to initiate crystallization of a supercooled melt at a predetermined temperature, which results in more reliable melting-point data.

3. FURNACE DESCRIPTION

Figure 2 shows the furnace with the ampoule in place. The mass of the heater is minimized by making it out of fused silica tubing whose wall thickness is reduced to about 1 mm by the spiral groove. The winding extends only 4 cm above and below the tip of the thermocouple. The ampoule rests on the thermocouple bead itself and is kept from tipping by the upper firebrick cover. A 3 cm wide steel strap (not shown), with a hole to admit the shaft of the ampoule, is screwed onto the Micarta base and holds the assembly together. Seeding is accomplished in the following way: prior to a thermal run, a small portion of charge is placed in the bulb which projects from the side of the tube (the temperature gradient is such that this material remains unmelted during the run). At the proper moment the furnace is tilted causing the solid material to drop into the melt.

The apparatus intentionally is not really a furnace in the sense of having a well defined ambient temperature, but is merely a radiant heater for the ampoule. The temperature of the ampoule is the only point of interest and it undoubtedly lags somewhat behind that of the Kanthal winding. The useful heater current is in the neighborhood of 1-3.5 amps, and must be adjusted individually for different temperatures and desired heating or cooling rates.

4. EXPERIMENTAL RESULTS

Calibration of the furnace system was performed with metals of known freezing points. All except Sb demonstrated no tendency to supercool and needed no seeding. Figure 3 shows some illustrative examples. The following observations are of interest:

1. In all cases, the heating arrest begins at or near the temperature of the cooling arrest, but the thermocouple temperature continues to rise slightly. Flat heating arrests are noted only rarely (Zn,Ge) but even then, the recorded melting points are about 1°C higher than the freezing points.

2. Cooling arrests may show a slight downslope, but are generally flat. For single-phase congruently melting substances, sloped arrests are due to partial response of the thermocouple to the changing environment outside of the ampoule. The extent of the slope probably increases with decreasing specific heat/unit volume of the sample substance and is caused by competing processes already mentioned above.

3. The experiment with Sb deserves a more detailed description: the initial flat cooling arrest was not allowed to go to completion so that it may be repeated with some solid still present in the melt. Thus, we note that the thermocouple can be heated even during an arrest, here by applying only 0.5 amps more current. However, a slight kink soon

afterwards indicates that complete fusion has probably occurred. The S-shaped curve afterwards simply indicates some fast maneuvering to achieve supercooling followed by a more gradual downslope to a temperature suitable for seeding. Although this was only 7.5°C below the initial arrest, it sufficed to depress the recorded freezing point by 0.5°C followed by a downslope of about 0.1°C/minute.

4. The recorded freezing points are high compared to the published values (numbers in parentheses). Average values obtained from duplicate runs of five standards are shown below:

TABLE I. CALIBRATION OF APPARATUS

Sample	M.P.	Recorded Arrests	Average	Δ
Pb	327.4	328.7, 329.3	329.0	+1.6
Zn	419.5	422.0, 421.4	421.7	+2.2
Sb	630.5	631.0, 632.0, 631.5	631.5	+1.0
Al	659.7	661.9, 661.8	661.9	+2.2
Ge	937.4	936.5, 936.0	936.3*	-1.1

The differences are probably due to the characteristics of the thermocouple. The previously mentioned sources of error cause low readings of freezing points which appears to be reflected only in the data for Ge where losses, e.g., by heat conduction through the thermocouple leads, may predominate due to the high temperature gradients. A new set of calibration points would be necessary for each new thermocouple.

*A 23-minute long constant heating arrest was obtained at 937°C.

Figure 4 shows thermal analyses of three sulfosalts. Here again, all cooling arrests are below the corresponding heating arrests. The "wiggle" in the generally flat heating arrest of TAS has been noted repeatedly on this and similar compositions. Owing to the rapid heating rate, the arrest is probably higher than it would normally occur. The cooling arrest is sluggish and did not occur at all at a seeding temperature of only 5°C below the freezing point. As it is (seed at 19°C below F.P.), the recorded temperature should probably be corrected by subtracting 1.6°C according to Table I (Pb). Hence, a good estimate for this particular sample would be 310 $\pm$ 1°C.

Reported DTA data for $TlBiTe_2$ are at 526°C (eutectic) and 539°C (pure compound). Our sample was known to contain at least a small amount of a second phase; thus, the ill defined arrests are easily explained. No conclusions can be drawn from the present data.

$CuSbS_2$ is an example of a sulfosalt compound that tends to supercool severely; the dashed curve represents a run in which spontaneous nucleation finally occurred 55°C below the reported melting point (553 $\pm$ 2°C). This was clearly too much for the equipment to handle as seen by the immediate steep downslope of the cooling arrest. This tracing is, however, instructive on how the current input was periodically adjusted so as to obtain a slow rate of cooling at all times, and the speed with which the apparatus can respond to adjustments of only 50 mA in heater current. The solid curve shows a repeated run with the same ampoule which was seeded at 18°C below the reported melting point. This

cooling arrest appears flat for about 4 minutes, but again, this figure should be corrected by subtracting 1-2°C as per Table I. Thus, the best estimate is probably 550.5 $\pm$ 1°C.

PbTe (not shown) melts at 923 $\pm$ 0.5°C. Our data of 923.5 and 924°C are from arrests which occur spontaneously after supercooling by 3.5°C and which remain flat for about 3 minutes. After adding 1.1°C (Table I, Ge), a good estimate is 925 $\pm$ 1°C.

5. CONCLUDING REMARKS

This initial study was concerned mainly with accuracy to evaluate the general performance of the apparatus. It is clear, however, that much more work is required before reliable estimates of systematic errors can be established which relate to parameters such as operating temperature, sample size, specific heat, and heating or cooling rates. In the meantime, it appears that the present equipment should be capable of determining the shape of phase relationships within a narrow range of compositions with a high degree of precision. This is emphasized for the data for $CuSbS_2$ and Tl_3AsSe_3. A new determination of Tl_3AsSe_3 melting relations will be presented in a separate report (G. W. Roland, in preparation).

6. ACKNOWLEDGMENTS

The author is grateful to Dr. G. W. Roland for helpful discussions, and to Mr. E. P. A. Metz for his valuable help in furnace construction and performance of the experimental work.

REFERENCE

1. G. W. Roland, J. P. McHugh, and J. D. Feichtner, J. of Electronic Mater. 3, 829 (1974).

PERMANENT RECORD BOOK ENTRIES

None.

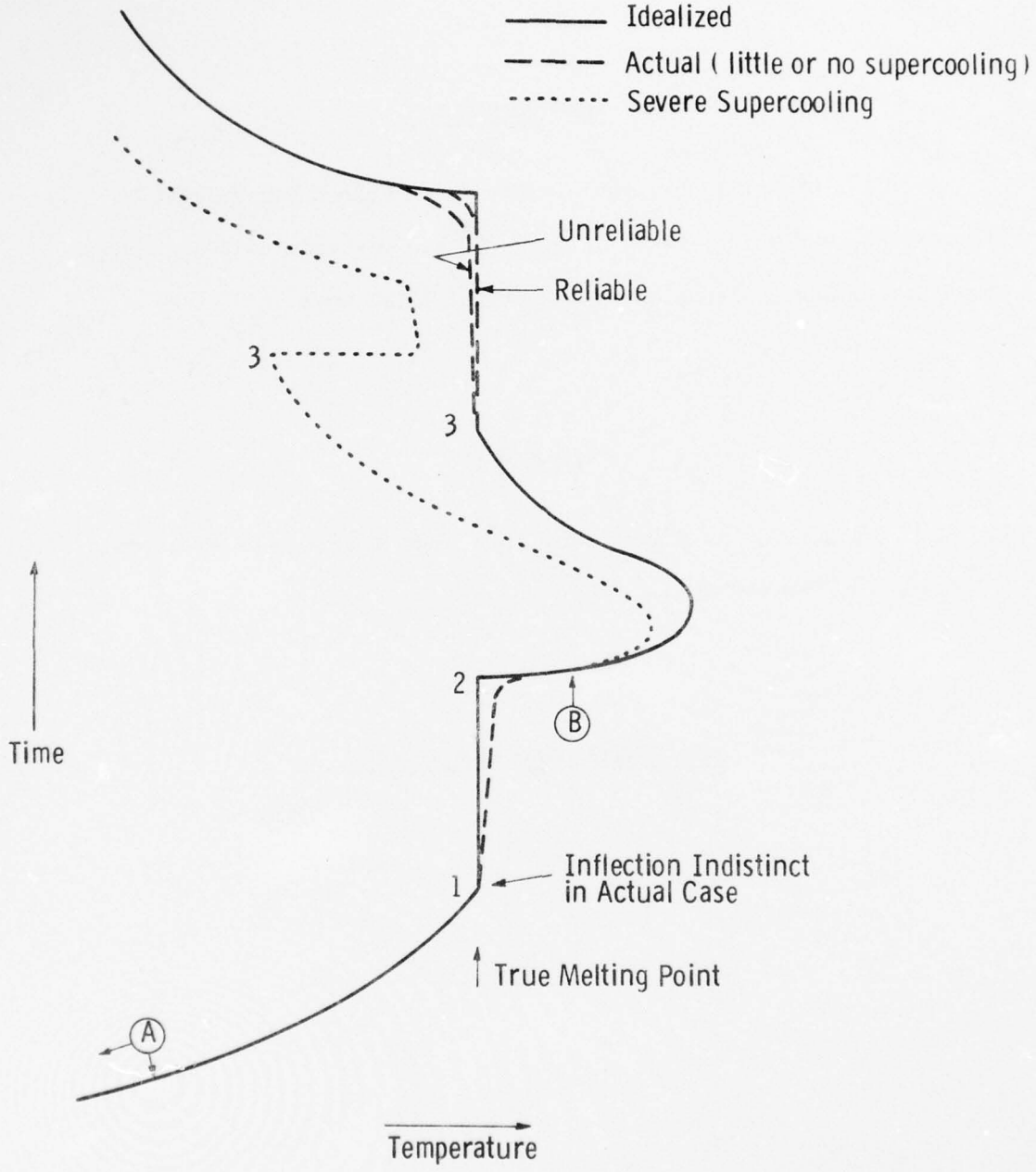

Fig. 1. Schematic representation of thermal arrests. Heater current is adjusted at points A and B so as to obtain suitable temperature/time slopes at points 1 and 3.

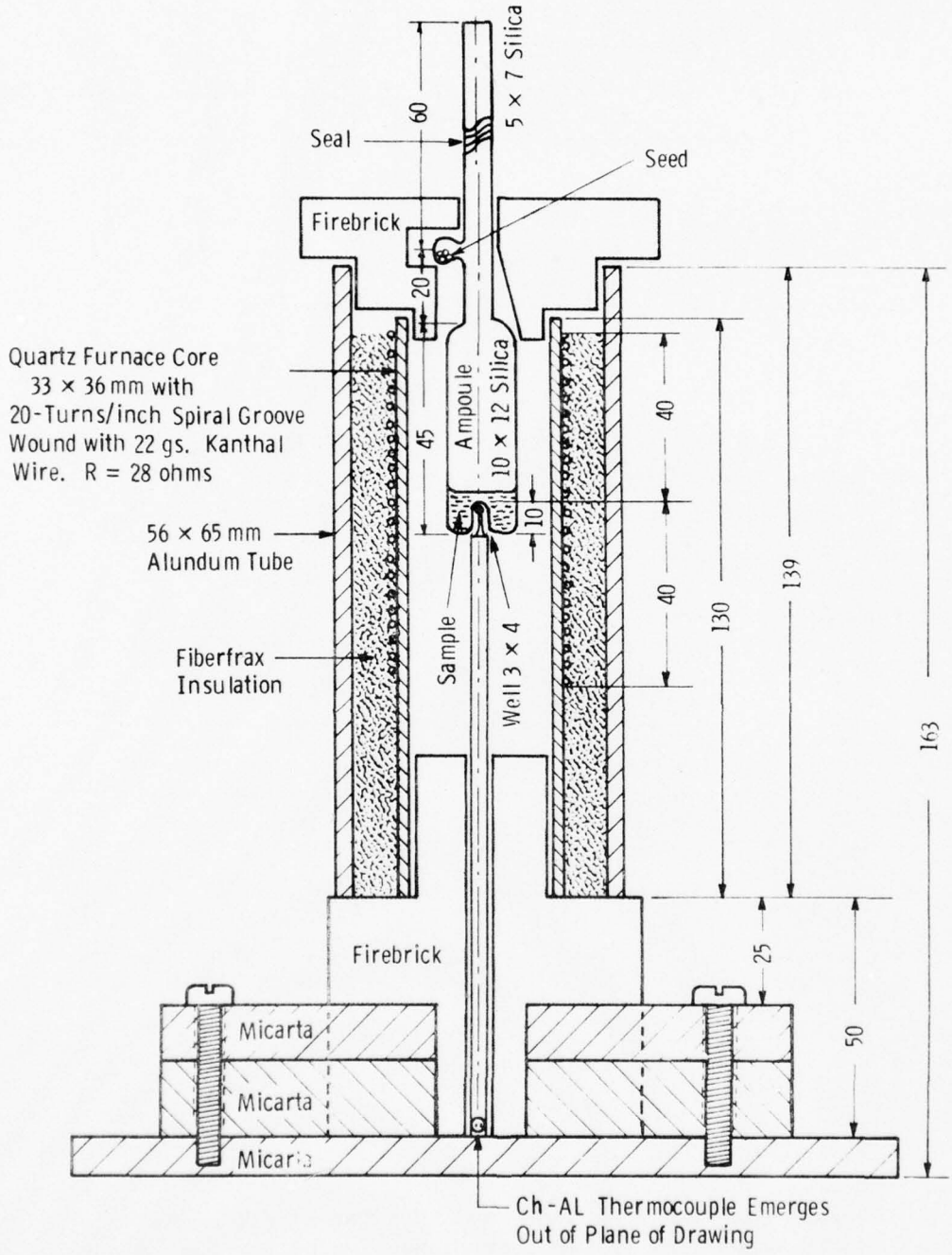

Fig. 2. Furnace with ampoule in place. Electrical connections of the heater core with the Variac lead between the Alundum tube and the upper and lower firebrick plugs.

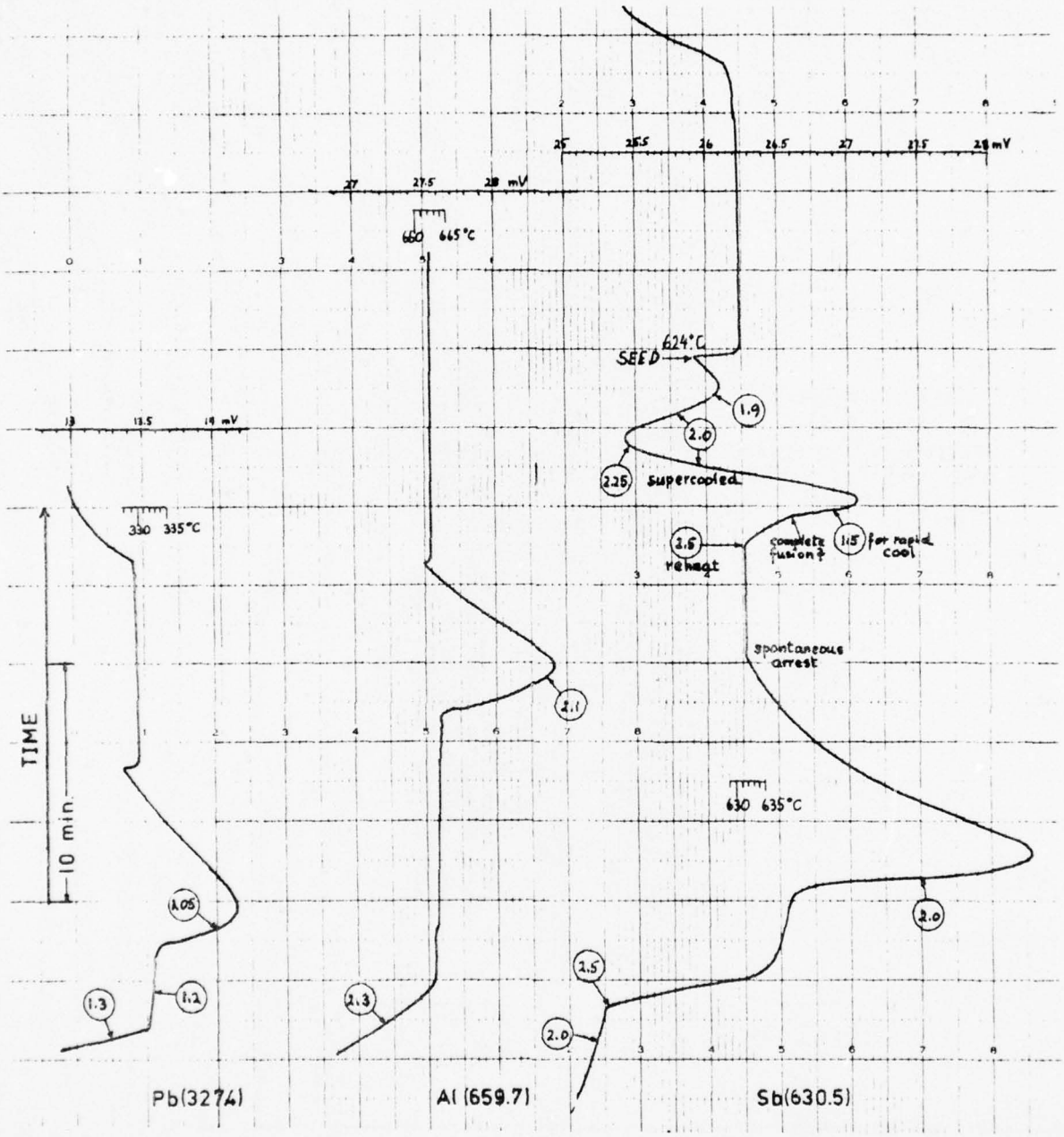

Fig. 3. Thermal analyses of Pb, Al, and Sb. The circled numbers denote amperes of heater current applied at the points shown by the arrows. The temperature scales denote published values for Chromel-Alumel, not the actual response of the thermocouple in use.

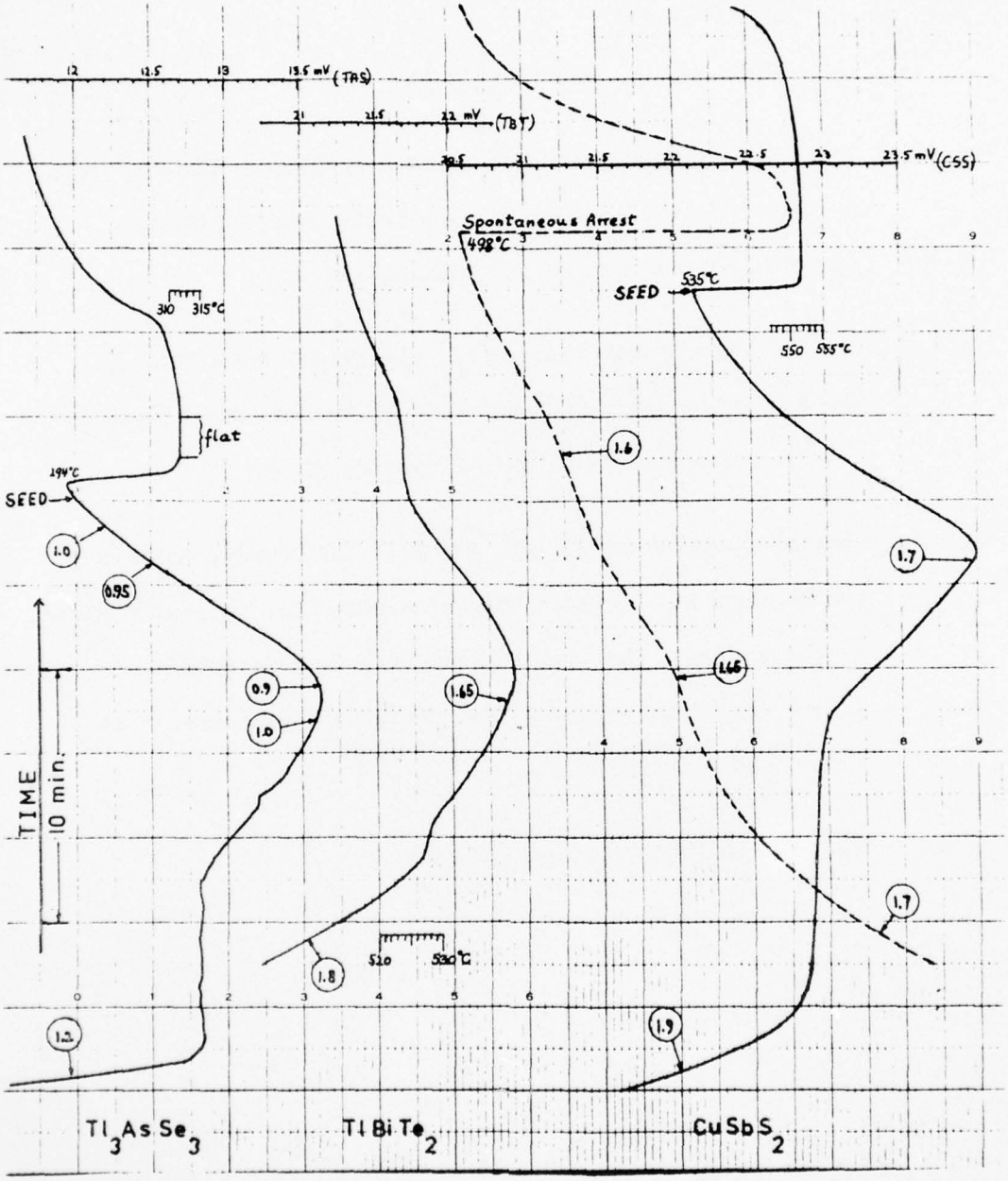

Fig. 4. Thermal analyses of some sulfosalts.

FIGURE CAPTIONS

Fig. 1. Schematic representation of thermal arrests. Heater current is adjusted at points A and B so as to obtain suitable temperature/time slopes at points 1 and 3.

Fig. 2. Furnace with ampoule in place. Electrical connections of the heater core with the Variac lead between the Alundum tube and the upper and lower firebrick plugs.

Fig. 3. Thermal analyses of Pb, Al, and Sb. The circled numbers denote amperes of heater current applied at the points shown by the arrows. The temperature scales denote published values for Chromel-Alumel, not the actual response of the thermocouple in use.

Fig. 4. Thermal analyses of some sulfosalts.

MISSION
of
Rome Air Development Center

RADC plans and conducts research, exploratory and advanced development programs in command, control, and communications (C^3) activities, and in the C^3 areas of information sciences and intelligence. The principal technical mission areas are communications, electromagnetic guidance and control, surveillance of ground and aerospace objects, intelligence data collection and handling, information system technology, ionospheric propagation, solid state sciences, microwave physics and electronic reliability, maintainability and compatibility.

Printed by
United States Air Force
Hanscom AFB, Mass. 01731